J. Fluid Mech. (1991), *vol.* 231, *pp.* 73–111
Printed in Great Britain

Spanwise pairing of finite-amplitude longitudinal vortex rolls in inclined free-convection boundary layers

By C. C. CHEN[1], A. LABHABI[1]†, H.-C. CHANG[1]‡ AND R. E. KELLY[2]

[1] Department of Chemical Engineering, University of Notre Dame, Notre Dame, IN 46556, USA

[2] Mechanical, Aerospace, and Nuclear Engineering, University of California, Los Angeles, CA 90024, USA

(Received 29 December 1989 and in revised form 27 February 1991)

Buoyancy-driven flow on a heated inclined plate can become unstable to static longitudinal roll instability at a critical distance, measured by $\tilde{R}_c$, from the leading edge. Experiments in water by Sparrow & Husar (1969) indicate that these rolls undergo a second transition further downstream such that adjacent rolls merge and their spanwise wavelength is doubled. We study this secondary bifurcation phenomenon here with a set of model equations by first constructing the full eigenspectrum and eigenfunctions with a Chebyshev–Tau spectral method and then deriving the pertinent amplitude equations. By stipulating that the dimensional cross-stream wavelength of the rolls remains constant beyond $\tilde{R}_c$, which is consistent with experimental observation, we show that the finite-amplitude primary rolls are destabilized by the $\frac{1}{2}$ subharmonic mode at another critical distance $\tilde{R}_{\frac{1}{2}}$ from the edge. This $\frac{1}{2}$ mode is shown to have an asymmetric spatial phase shift of $\frac{1}{2}\pi$ relative to the original 1 mode of the primary rolls, thus explaining the unique dislocation of tracer streaks after the rolls coalesce in the experiments. Also consistent with experimental observation is the theoretical result that the merged rolls are annihilated downstream by a saddle-node bifurcation before further wavelength doubling can occur. Simple amplitude criteria and critical distances from the leading edge for the various transitions are derived and compared to experimental values.

1. Introduction

We are concerned with the nonlinear development of longitudinal vortex rolls in natural convection boundary layers on heated inclined plates as shown schematically in figure 1. These rolls occur as a result of a non-zero buoyancy force in the direction normal to the plate. Consequently, vertical or near-vertical plates are stable to this roll instability. The near-vertical plates, however, can be unstable to Tollmien–Schlichting-type wave instability (Lloyd & Sparrow 1970). The appearance of longitudinal vortices on inclined plates in many new industrial processes such as chemical vapour deposition has recently revived interest in this classical problem (Jensen 1987). However, except for numerical simulations of buoyancy-driven

† Present address: Chemical Engineering Department, Ecole Nationale de L'Industrie Minerale B. P 753, Agdal-Rabat, Morocco.

‡ Author to whom correspondence should be addressed.

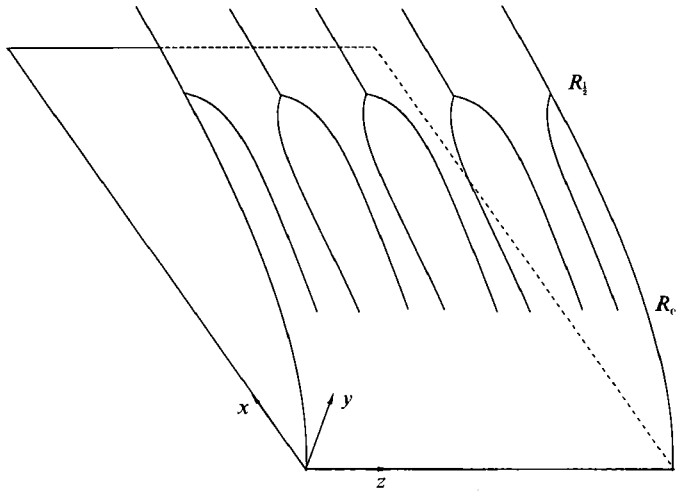

FIGURE 1. Schematic of roll pairing in free-convection boundary layers. The longitudinal vortices develop at R_c and coalesce at $R_{\frac{1}{2}}$. Note the dislocation of the merged rolls relative to the primary ones.

vortices in complex geometries (Yang 1988), nonlinear evolution of these vortices after their inception has not been studied for the simple inclined plate geometry. Sparrow & Husar (1969) first observed in water a now well-known wavelength-doubling phenomenon of these longitudinal rolls at a critical distance from their inception. Gilpin, Imura & Cheng (1978) have also observed the same phenomenon in water for a heated Blasius boundary layer. As shown in figure 1, adjacent rolls merge abruptly after this transition and double their cross-stream wavelength. The merged rolls are also shifted from the primary rolls so that a unique dislocation of the tracer streaks, which occupy the sides of the rolls where the flow is in the normal direction away from the plate, are seen in Sparrow & Husar's experiments. This is shown schematically in figure 1. Further downstream, the tracer experiments of Sparrow & Husar indicate that the merged rolls are dissipated by turbulence without further wavelength doubling. The merging of adjacent rolls and the doubling of wavelength occur abruptly and discontinuously. Prior to and after the transition, the wavelengths remain extremely regular over relatively long distances. Hence, a wavelength adjustment mechanism arising from growth of the boundary-layer thickness such as occurs for Tollmien–Schlichting waves is not responsible for the coalescence. Such a mechanism would stipulate a slow and continuous increase of the cross-stream wavelength without merging or dislocation. A probable cause for the pairing phenomenon is the sudden destabilization of the finite-amplitude rolls by subharmonic disturbances. New rolls with twice the wavelength then bifurcate at the transition point, thereby allowing the convection rolls to have an aspect ratio more suitable to a larger boundary-layer thickness. We shall develop a secondary bifurcation theory here to explain the pairing phenomenon and the subsequent dissipation of the merged rolls.

When a system is unbounded in a particular direction, the corresponding spectrum, parameterized by the wavenumber in the unbounded direction, is continuous and an entire band of unstable wavenumbers exists beyond criticality. In many systems, such as the present one, the possible wavenumbers selected out of this band are only a subset of the entire band. The other wavenumbers are unstable to disturbances with slightly different wavenumbers and are hence not selected. This

sideband instability was first studied by Eckhaus (1963) who showed that monochromatic rolls in a non-dispersive system with wavenumbers α within the range

$$(\alpha_- - \alpha_c)/\sqrt{3} < \alpha - \alpha_c < (\alpha_+ - \alpha_c)/\sqrt{3}, \tag{1.1}$$

where α_c is the critical wavenumber and $\alpha_\pm$ are the two neutral wavenumbers which bound all linearly unstable modes, are stable to sideband disturbances near criticality. We have recently extended the Eckhaus bound to dispersive systems and away from criticality (Cheng & Chang 1990). However, as we shall show subsequently, the present roll instability is non-dispersive and the finite-amplitude primary roll is stable to sideband disturbances according to the Eckhaus bound. This is consistent with the patterns observed by Sparrow & Husar which show very little sideband modulation. Another instability can also occur for convective rolls in shear flows as the Rayleigh or Reynolds number increases beyond the critical value for onset of rolls. Clever, Busse & Kelly (1977) have shown that, for a Couette flow heated from below, the convective rolls can be destabilized by a streamwise wavy instability which occurs slightly above criticality. However, since this wavy instability occurs first for infinite-wavelength disturbances, it is less likely to occur in non-parallel boundary-layer flows. There are indications that this wavy instability resembles one type of instability of Görtler vortices (see figure 14(*c*) of Swearingen & Blackwelder 1987) and so might occur for convective instabilities in low-Prandtl-number fluid boundary-layer flows. Beside the sideband and wavy instabilities, subharmonic instability also seems to be prevalent for finite-amplitude monochromatic waves. There have been some recent studies of subharmonic excitation in many different systems such as sheared gravity–capillary waves (Janssen 1986) and horizontal fluid layers heated from below (Busse & Or 1986). Vortex pairing in a free shear layer is, however, the most studied example of a system whose critical monochromatic wave is unstable to a subharmonic instability such that adjacent vortices coalesce in a wavelength-doubling transition after the critical mode has grown to a critical and finite amplitude. This phenomenon was first observed by Sato (1959), and Kelly (1967) derived the pertinent amplitude equations to show that the subharmonic mode is excited through nonlinear interaction. He also predicted the excitation of the $\frac{3}{2}$ mode which was later observed. Monkewitz (1988) has recently extended the amplitude equations to account for spatial growth of the disturbances and frequency mismatch. There is hence considerable interest in constructing a general subharmonic instability theory, as in the sideband stability theory, to understand the nonlinear wavenumber selection process in an unbounded system. In an inviscid shear layer without gravity stratification, however, the Kelvin–Helmholtz instability dictates that all streamwise wavenumbers between zero and the maximum-growing one are linearly unstable. Consequently, all subharmonics are unstable and higher subharmonics will eventually be excited even though the current theories only consider the first subharmonic. Thomas (1990) has observed some of these higher subharmonics in his experiments with planar jets and one generally expects a sequence of coalescence. In the present natural convection problem in a boundary layer, the band of unstable cross-stream wavenumbers is bounded away from zero. Consequently, the higher subharmonics are linearly stable except at distances very far from the leading edge. We shall demonstrate in our analysis that the merged rolls have already dissipated via a unique saddle-node bifurcation at such distances. As a result, excitation of the stable subharmonics is far more difficult in the present problem and higher subharmonic modes have never been observed. Also, for an inviscid shear layer, the coalesced vortices grow unarrested in space and time.

In the present problem, through interaction with the stable subharmonic modes, finite-amplitude saturated rolls are predicted and observed both prior to and after wavelength doubling. There are hence fundamental differences in the excitation mechanism of the subharmonics in these two systems.

There is a large body of literature on the linear stability of the flow under consideration (see the most recent review by Gebhart *et al.* 1988). After Yang (1960) derived the similarity solution to the steady-state vertical-plate problem, Haaland & Sparrow (1973) examined the growth of longitudinal roll disturbances on inclined plates with a parallel-flow theory. In their similarity analysis of the main flow, the pressure gradient term in the streamwise direction is neglected and the only driving force for flow parallel to the plate is the corresponding component of the buoyancy force. This approximation, which is valid for inclination angles no more than 45° from the vertical, allows them to carry out a similarity analysis for the main flow of the inclined plate which is identical to Yang's solution of the vertical case. By assuming static instability (viz. the principle of exchange of stability), they showed that the basic flow for these plates destabilizes at $R = 23.5/\tan\theta$ for a Prandtl number Pr of 6.7, where R is the local Reynolds number measured from the edge defined in (2.10a) and θ is the inclination angle from vertical. Their computation was later improved by Chen & Tzuoo (1982) who also examined the case of horizontal and inclined plates. The assumption of exchange of stability, which is based on purely physical arguments since the eigenvalue problem is not self-adjoint, is also imposed in Chen & Tzuoo's computations. Quantitative agreement between theory and experiment for the onset of roll instability is still unsatisfactory, with the observed transition from the basic flow to the primary rolls occurring downstream of the predicted station. Attempts to remedy this discrepancy by considering the amplification of small disturbances have been proposed (Iyer & Kelly 1974). Probably experiments using controlled disturbances (as done regularly for Tollmien–Schlichting instability) will have to be performed before theoretical and experimental results can be compared definitively. Moreover, for very small θ, the Tollmien–Schlichting travelling wave instability with streamwise variation but no spanwise dependence seems to be more unstable than the roll instability (Lloyd & Sparrow 1970). This has also been theoretically confirmed by Hwang & Cheng (1973), Haaland & Sparrow (1973), Kahawita & Meroney (1974), Iyer & Kelly (1974) and Tzuoo, Chen & Armaly (1985) for various Prandtl numbers Pr and inclination angles θ. Kahawita & Meroney predicted that at $Pr = 0.72$, the wave instability becomes dominant for $\theta < 17°$ and Iyer & Kelly found that for water ($Pr = 6.7$), the cross-over angle based on a parallel flow model is $\theta = 4°$. Tzuoo's *et al.*'s computations which allow for some non-parallel effects show larger cross-over angles. Experimental values of Lloyd & Sparrow (1970) for water are between 14° and 17°. There is also a large body of literature on periodically forced two-dimensional Tollmien–Schlichting waves (see the review by Gebhart & Mahajan 1982) which is not pertinent to the roll instability problem studied here.

We shall here focus on nonlinear subharmonic instability of the longitudinal rolls and the evolution of the merged rolls. Interaction between the roll and wave instabilities will be reported in a later manuscript. In general, interaction between these two modes is most pronounced near the cross-over θ when the critical Reynolds number R_c for both instabilities become identical (see studies on interactions between Görtler vortices and Tollmien–Schlichting waves in curved channels by Daudpota, Hall & Zang (1988), between temperature-driven and solute-driven instabilities in the doubly-diffusive Marangoni problem by Ho & Chang (1988) and

between even and odd convective patterns in Taylor–Bénard instability in a Hele-Shaw cell by Hwang & Chang (1989)). Also, computations by Tzuoo *et al.* (1985) and experimental observations (Sparrow & Husar 1969) show that the dimensional streamwise wavelength of the wave instability is much longer than the spanwise wavelength of the roll instability. Consequently, if the growth rate of the wave instability is small, the roll instability will most likely evolve independently from the wave instability even for near-vertical plates where the wave instability destabilizes first. This allows a simplifying modified parallel-flow approximation to be made, as will be discussed later. It should also be mentioned that Benney (1960) and Benney & Lin (1960) have shown that two-dimensional finite-amplitude travelling waves in shear flows can be unstable to three-dimensional disturbances such that longitudinal rolls are created. It is unlikely that the observed vortices in the present problem are formed from finite-amplitude Tollmien–Schlichting travelling waves since the basic flow itself is more susceptible to roll instability than the wave instability except at very small θ.

The major obstacle to the nonlinear analysis is the resolution of the eigenfunctions in the normal semi-infinite direction. To obtain the amplitude equations, not only the critical eigenmode but also several of its subharmonics and superharmonics need to be constructed since finite-amplitude rolls and their stability are caused by nonlinear interaction among these modes. The conventional shooting method which constructs the critical mode at onset would be inadequate for this task. We use a Tau-spectral method here for the eigenvalue problem in semi-infinite domains and demonstrate its accuracy with a convergence study.

In §2, we derive the nonlinear governing transport equations for roll instability by imposing the modified parallel-flow approximation. The resulting equations are essentially nonlinear extensions of Haaland & Sparrow's linear theory for plates with θ less than 45°. In §3, we solve the full eigenspectrum of the linear stability problem without assuming the principle of exchange stability as previous workers. Although complex eigenvalues were found, the most unstable one is always real. We stipulate that the rolls retain the dimensional spanwise wavelength of the fastest-growing linear mode, which is consistent with experimental data. In §4, we derive the amplitude equations describing the quadratic interaction between the fundamental, subharmonic and superharmonic spanwise modes of these rolls. The amplitude equations are solved numerically for increasing values of R. It is shown that the fundamental mode interacts with its overtone to form a finite-amplitude standing roll which bifurcates supercritically at the critical Reynolds number R_c. When the amplitude of this primary roll exceeds a critical value, it becomes unstable to the linearly unstable $\frac{1}{2}$ mode of the main flow such that the bifurcating rolls downstream have twice the wavelength of the primary rolls. The precise shift dislocation is also obtained from our theory. After the rolls coalesce, they disappear chaotically further downstream via a saddle-node bifurcation and no further wavelength doubling occurs. Even this prediction is in qualitative agreement with the experiments of Sparrow & Husar (1969). In §5, we augment the numerical solution with a bifurcation analysis to obtain analytical estimates of the transitions and their onset conditions. The analysis also reveals that the shift between the merged and unmerged rolls is caused by a particular nonlinear coefficient in the amplitude equations. The results are summarized in §6.

2. Formulation

By imposing the Boussinesq approximation, the equations of motion and the energy equation are (Gebhart *et al.* 1988; Haaland & Sparrow 1973)

$$\partial V/\partial \hat{t} + V\cdot\nabla V = -1/\rho\,\nabla p - \beta g(T-T_\infty) + \nu\nabla^2 V, \tag{2.1a}$$

$$\partial T/\partial \hat{t} + V\cdot\nabla T = \alpha\nabla^2 T, \tag{2.1b}$$

$$\nabla\cdot V = 0, \tag{2.1c}$$

where T_∞ is the ambient temperature, β the expansion coefficient, ν the kinematic viscosity and α the thermal diffusivity. We shall simplify these equations by using the boundary-layer approximation for the basic flow and a model set of equations for the disturbance in which the dependence of the perturbations on the streamwise x-coordinate is ignored. The linearized version of this model has been proposed to extend the conventional parallel-flow stability theory so as to include the normal component of the disturbance velocity entirely (Haaland & Sparrow 1973). For homogeneous shear flows, use of this model gives rise to the 'modified' Orr–Sommerfeld equation, and some refer to its use as a modified parallel-flow assumption. Like strict parallel-flow theories, it allows the construction of a local Orr–Sommerfeld equation for each point along the boundary layer, and the Reynolds number, which is actually a measure of the distance from the edge, then becomes a convenient control parameter in the equation. Haaland & Sparrow (1973), Kahawita & Meroney (1974) and Chen & Tzuoo (1982) have all used such an approximation to study the linear stability of the present flow in regard to the thermally driven instability. For this particular flow, its use allows the fact that the velocity component normal to the plate is *inwards* at the edge of the boundary layer to be taken into account, which is vital to the analysis of long-wavelength disturbances. Gebhart & Mahajan (1982) and Tzuoo *et al.* (1985) also employed the same approximations to study streamwise Tollmien–Schlichting waves in the same flow. The analogous parallel-flow linear theories for spanwise Görtler instability have been scrutinized by Hall (1983). For spanwise vortex wavelengths equal to or larger than the boundary-layer thickness, he shows that the parallel-flow theory does not yield the proper limiting behaviour of the vortex disturbances at the upper edge of the boundary layer. Not surprisingly, when he numerically integrates the complete linearized equations of motion, he finds that the onset position of very long vortex disturbances is dependent on the form of the initial disturbance and can be far from the unique prediction of the parallel-flow theory. However, the numerical result in his figure 7 also shows that at $\alpha x^{\frac{1}{2}} \sim 2$, where α is the dimensionless spanwise wavenumber and x is the dimensionless streamwise coordinate that the point when the spatial growth rate vanishes and both are scaled with respect to the boundary-layer thickness. His numerical results for the onset location for various disturbances are within 20% of the parallel-flow prediction, and the growth rates all approach the parallel-flow result at even larger values of $\alpha x^{\frac{1}{2}}$. Since x is typically large (~ 50), this shows that the parallel-flow theory remains a reasonably good approximation, as far as the prediction of onset is concerned, even when the spanwise wavelength is the same order as the boundary-layer thickness. It is when the vortex wavelength is much longer than the boundary-layer thickness that the parallel-flow theories fail. Agreement with experimental measurements is, however, another matter and, generally speaking, Hall's numerical results for onset are well below the experimental data. All buoyancy-induced rolls in the experiments of Sparrow & Husar (1969) and Gilpin *et al.* (1978) have dimensions within the range where the parallel-flow theory

is reasonably valid. Moreover, unlike Görtler instability, the streamwise velocity vanishes rapidly away from the wall in a free convection boundary layer. This diminishes the effect of streamwise convection and renders parallel-flow theory more appropriate. We shall show that, in the present problem, the parallel-flow approximation provides a prediction of the critical wavenumber that is accurate to within 25%. As in the Görtler instability studied by Hall (1983), the prediction of the critical distance from the edge is less accurate with errors sometimes exceeding 100% (as is also true for the results of Haaland & Sparrow 1973 and Chen & Tzuoo 1982). The quantitative success (less than 30% error) of the parallel-flow approximation in analysing the stability of the Blasius boundary layer is hence not duplicated here. Nevertheless, the linear stability results of Chen & Tzuoo (1982) indicate that the qualitative effects of the various parameters on the stability of the problem are still faithfully reproduced. We will retain the modified parallel-flow approximation here in order to simplify the analysis. A direct attack on (2.1) is still not feasible numerically. However, we shall present quantitative comparisons of our results to the experimental values as often as possible in order to test the accuracy of the model equations.

For the steady-state problem, if the usual boundary-layer approximations are introduced and if the pressure gradient in the x-direction is neglected, a similarity transform can be carried out to reduce the order of equation (2.1) (see Haaland & Sparrow 1973). The analysis yields

$$F''' + 3FF'' - 2F'^2 + \phi = 0, \tag{2.2a}$$

$$\phi'' + 3PrF\phi' = 0, \tag{2.2b}$$

with boundary conditions

$$F(0) = F'(0) = F'(\infty) = \phi(\infty) = 0, \tag{2.2c}$$

$$\phi(0) = 1, \tag{2.2d}$$

for the isothermal plate problem. In (2.2), the derivatives (denoted by a prime) are with respect to the similarity variable $\eta = y/h(x)$ where

$$h(x) = x^{\frac{1}{4}}/\kappa, \tag{2.3a}$$

$$\kappa = [\beta g \cos\theta (T_w - T_\infty)/4\nu^2]^{\frac{1}{4}}, \tag{2.3b}$$

$F(\eta)$ is related to the steady-state stream function ψ^*,

$$F(\eta) = \psi^*/4\nu\kappa x^{\frac{3}{4}} \tag{2.3c}$$

and $\phi(\eta)$ is the dimensionless steady-state temperature

$$\phi(\eta) = (T^* - T_\infty)/(T_w - T_\infty), \tag{2.3d}$$

where T^* is the dimensional steady-state temperature and T_w is the plate temperature which is assumed to be a constant. The coordinates x and y respectively denote streamwise distance from the edge of the plate and normal distance from the plate. The two-dimensional basic flow is obtained by solving (2.2) with a standard shooting method which iterates $\phi'(0)$ and $F'(0)$ until the two conditions at $\eta = \infty$ in (2.2) are satisfied. The iterations are stopped when the Newton–Raphson method has converged to the fifth decimal place. The resulting values can then be used to compute the basic temperature profile $T^*(x, y)$ and the basic flow

$$U^*(x, y) = \frac{\partial \psi^*}{\partial y}, \quad V^*(x, y) = -\frac{\partial \psi^*}{\partial x}. \tag{2.4}$$

Introducing the deviation variables

$$V = V^* + v(y, z, \hat{t}) = \begin{pmatrix} U^* \\ V^* \\ 0 \end{pmatrix} + \begin{pmatrix} u \\ v \\ w \end{pmatrix}, \tag{2.5a}$$

$$T = T^* + \tau(y, z, \hat{t}), \tag{2.5b}$$

$$\psi = \psi^* + \hat{\psi}(y, z, \hat{t}), \tag{2.5c}$$

neglecting the x-dependence of the deviation variables in accordance with the modified parallel-flow approximation and further assuming that the disturbance grows temporally instead of spatially in the downstream direction, one obtains from (2.1) after taking the curl of the equation of motion

$$\frac{\partial \omega}{\partial \hat{t}} + V^* \frac{\partial \omega}{\partial y} + \omega \frac{\partial V^*}{\partial y} - \frac{\partial \hat{\psi}}{\partial z}\frac{\partial \omega}{\partial y} + \frac{\partial \hat{\psi}}{\partial y}\frac{\partial \omega}{\partial z} = -g\beta \sin\theta \frac{\partial \tau}{\partial z} + \nu \nabla^2 \omega, \tag{2.6a}$$

$$\frac{\partial u}{\partial \hat{t}} + V^* \frac{\partial u}{\partial y} - u \frac{\partial V^*}{\partial y} - \frac{\partial \hat{\psi}}{\partial z}\frac{\partial U^*}{\partial y} - \frac{\partial \hat{\psi}}{\partial z}\frac{\partial u}{\partial y} + \frac{\partial \hat{\psi}}{\partial y}\frac{\partial u}{\partial z} = g\beta \cos\theta \tau + \nu \nabla^2 u, \tag{2.6b}$$

$$\frac{\partial \tau}{\partial \hat{t}} + u \frac{\partial T^*}{\partial x} - \frac{\partial \hat{\psi}}{\partial z}\frac{\partial T^*}{\partial y} + V^* \frac{\partial \tau}{\partial y} - \frac{\partial \hat{\psi}}{\partial z}\frac{\partial \tau}{\partial y} + \frac{\partial \hat{\psi}}{\partial y}\frac{\partial \tau}{\partial z} = \alpha \nabla^2 \tau, \tag{2.6c}$$

where ω is the vorticity component in the x-direction for the two-dimensional disturbance flow field

$$\omega(y, z) = \frac{\partial w}{\partial y} - \frac{\partial v}{\partial z} = \nabla^2 \hat{\psi}(y, z), \tag{2.7a}$$

and

$$w = \left(\frac{\partial \hat{\psi}}{\partial y}\right), \quad v = -\left(\frac{\partial \hat{\psi}}{\partial z}\right) \tag{2.7b}$$

and the Laplacian operator ∇^2 in (2.6) and (2.7a) is a two-dimensional one with respect to y and z.

The neglect of the x-dependence in the modified parallel-flow approximation of (2.5) and the retention of nonlinear terms involving the deviation variables require some justification concerning the magnitudes of the streamwise lengthscale and the disturbance field. We shall sketch a leading-order multi-scale derivation of (2.6) here. We first allow x-dependence in the deviation variables of (2.5) but stipulate that the dependence is weak such that the deviation variables are functions of the scaled x-coordinates $x_1 = \epsilon_1 x$. This weak dependence of both the disturbance and the main flow on x is evident from literature reports. The boundary-layer thickness near the first onset of rolls is of the order of 0.5 cm while the transition of interest here typically occurs about 5 cm from the edge. Even in the case of the vertical plate with strong streamwise Tollmien–Schlichting instability, the disturbance usually evolves in the x-direction with a characteristic lengthscale of 5 cm (Szewczyk 1962). In comparison, the cross-stream wavelength is about 0.5 cm. These characteristic scales yield an ϵ_1 of lower than 0.1, which renders the parallel-flow approximation a reasonable one. We also stipulate that the disturbance variables have an amplitude of $O(\epsilon_2)$. Upon substituting such deviation variables into (2.1) and omitting terms of orders $O(\epsilon_1 \epsilon_2)$, $O(\epsilon_1^2)$ and higher, (2.6) is obtained. Since we are retaining the $O(\epsilon_2^2)$ nonlinear terms, this then stipulates that $\epsilon_1 \ll \epsilon_2$. For example, an order assignment of $\epsilon_2 \sim O(\epsilon_1^{\frac{1}{2}})$ would be appropriate. This then allows us to add the nonlinear terms to the linearized modified parallel-flow equations of the earlier studies. The neglected

higher-order terms in ϵ_1 in the modified parallel-flow approximation are all linear while the nonlinear terms are retained in (2.6). Consequently, the nonlinear interaction phenomenon should be modelled reasonably well, although the prediction of the transition points may be compromised. Indeed, in his analysis of the onset of Rayleigh–Bénard convection in a fluid layer of slowly increasing depth, Walton (1982) demonstrated that a sharp bifurcation does not occur near the 'critical' condition. However, for Rayleigh numbers in excess of the usual critical value, the amplitude of the convection cells approaches asymptotically the result for a constant-depth layer, namely with amplitude proportional to $[Ra(x)-Ra_c]^{\frac{1}{2}}$, where Ra is the Rayleigh number. Because we are mainly interested in supercritical phenomena, we take the view that a parametric dependence upon x via $R(x)$ is the item of central importance and so do not develop equations valid only in the immediate vicinity of R_c.

Equation (2.6) can be further simplified by scaling the deviation temperature with T_w-T_∞, the time with $h^2(x)/\nu$ and the deviation velocities with the characteristic velocity $\bar{u}(x) = 4\nu\kappa x^{\frac{1}{2}}$ to yield

$$\frac{\partial u}{\partial t} = u_{\eta\eta}+u_{\delta\delta}-V^*u_\eta+V^{*\prime}u+RF''f_\delta+\tau+R[f_\delta u_\eta-f_\eta u_\delta], \tag{2.8a}$$

$$\frac{\partial \omega}{\partial t} = \omega_{\eta\eta}+\omega_{\delta\delta}-V^*\omega_\eta-V^{*\prime}\omega-\tan\theta\,\tau_\delta+R[f_\delta\omega_\eta-f_\eta\omega_\delta], \tag{2.8b}$$

$$\frac{\partial \tau}{\partial t} = \frac{1}{Pr}(\tau_{\eta\eta}+\tau_{\delta\delta})-V^*\tau_\eta+R\phi' f_\delta+\eta\phi' u+R[f_\delta\tau_\eta-f_\eta\tau_\delta], \tag{2.8c}$$

$$\omega = f_{\eta\eta}+f_{\delta\delta}, \tag{2.8d}$$

$$V^* = \eta F'-3F, \tag{2.8e}$$

where the convective nonlinear terms are contained in the square brackets and prime denotes derivative with respect to η. The variable δ is the scaled cross-stream coordinate

$$\delta = z/h(x) \tag{2.9a}$$

and t is the scaled time coordinate

$$t = \nu\hat{t}/h^2(x). \tag{2.9b}$$

The dimensionless parameter R is the local Reynolds number, representing the normalized distance from the edge

$$R = \bar{u}(x)\,h(x)/\nu = 4\kappa x^{\frac{3}{4}} \tag{2.10a}$$

and $f(\eta,\delta,t)$ is the scaled deviation stream function

$$f = \hat{\psi}/(\bar{u}(x)\,h(x)). \tag{2.10b}$$

Equation (2.8) is subjected to the non-slip and isothermal boundary conditions at the wall and vanishing velocity and thermal disturbances far from the wall

$$u = \tau = f = f_\eta = 0 \quad \text{at} \quad \eta = 0 \text{ and } \infty. \tag{2.11}$$

The linear part of (2.8) can be further simplified if the following transformation introduced by Haaland & Sparrow is imposed to scale away explicit θ-dependence in the linear terms:

$$\tilde{\tau} = \tau\tan\theta, \quad \tilde{u} = u\tan\theta, \quad \tilde{R} = R\tan\theta \tag{2.12}$$

such that (2.8) becomes

$$\frac{\partial \tilde{u}}{\partial t} = \tilde{u}_{\eta\eta} + \tilde{u}_{\delta\delta} - V^*\tilde{u}_\eta + V^{*\prime}\tilde{u} + \tilde{R}F''f_\delta + \tilde{\tau} + \frac{\tilde{R}}{\tan\theta}[f_\delta \tilde{u}_\eta - f_\eta \tilde{u}_\delta], \tag{2.13a}$$

$$\frac{\partial \omega}{\partial t} = \omega_{\eta\eta} + \omega_{\delta\delta} - V^*\omega_\eta - V^{*\prime}\omega - \tilde{\tau}_\delta + \frac{\tilde{R}}{\tan\theta}[f_\delta \omega_\eta - f_\eta \omega_\delta], \tag{2.13b}$$

$$\frac{\partial \tilde{\tau}}{\partial t} = \frac{1}{Pr}(\tilde{\tau}_{\eta\eta} + \tilde{\tau}_{\delta\delta}) - V^*\tilde{\tau}_\eta + \tilde{R}\phi' f_\delta + \eta\phi'\tilde{u} + \frac{\tilde{R}}{\tan\theta}[f_\delta \tilde{\tau}_\eta - f_\eta \tilde{\tau}_\delta], \tag{2.13c}$$

$$\omega = f_{\eta\eta} + f_{\delta\delta}, \tag{2.13d}$$

with boundary conditions

$$\tilde{u} = \tilde{\tau} = f = f_\eta = 0 \quad \text{at} \quad \eta = 0 \text{ and } \infty. \tag{2.14}$$

We note that transformation (2.12) becomes singular for the vertical case $\theta = 0°$. In fact, longitudinal vortices do not form on vertical plates because of the lack of normal buoyancy force. If the nonlinear and time-dependent terms of (2.8) are omitted, it reduces to the static disturbance equations of Haaland & Sparrow (1973).

3. Eigenspectrum

Since δ and t do not appear explicitly in the linear portion of (2.13), a standard normal mode expansion is permissible for the spanwise direction,

$$\begin{pmatrix} \tilde{u} \\ \omega \\ \tilde{\tau} \\ f \end{pmatrix} = \begin{pmatrix} \hat{u}(\eta) \\ \hat{\omega}(\eta) \\ \hat{\tau}(\eta) \\ \hat{f}(\eta) \end{pmatrix} e^{i\alpha\delta + \lambda t}, \tag{3.1}$$

where α is the dimensionless wavenumber in the spanwise direction. Substitution of (3.1) into (2.13) then yields the eigenvalue problem

$$\tilde{\mathbf{L}} \begin{pmatrix} \hat{u} \\ \hat{\omega} \\ \hat{\tau} \end{pmatrix} = \lambda \begin{pmatrix} \hat{u} \\ \hat{\omega} \\ \hat{\tau} \end{pmatrix}, \tag{3.2}$$

where $\tilde{\mathbf{L}}$ is a differential-integral operator parameterized by the spanwise wavenumber α, the Prandtl number Pr and the normalized Reynolds number $\tilde{R}$ (note that θ has been scaled away in the linear problem),

$$\tilde{\mathbf{L}} = \begin{pmatrix} \mathrm{D} + V^{*\prime} & \alpha\tilde{R}F''\mathrm{L}^{-1} & 1 \\ 0 & \mathrm{D} - V^{*\prime} & \alpha \\ \eta T^{*\prime} & \alpha\tilde{R}T^{*\prime}\mathrm{L}^{-1} & \dfrac{1}{Pr}\mathrm{D} \end{pmatrix} \tag{3.3}$$

The operator D denotes viscous (conduction) and convective terms for momentum (energy) balance in the normal and spanwise directions

$$\mathrm{D} = \frac{\mathrm{d}^2}{\mathrm{d}\eta^2} - \alpha^2 - V^*(\eta)\frac{\mathrm{d}}{\mathrm{d}\eta} \equiv \mathrm{L} - V^*(\eta)\frac{\mathrm{d}}{\mathrm{d}\eta} \tag{3.4}$$

and L^{-1} denotes the inverse of the viscous operator

$$\mathrm{L} = \frac{\mathrm{d}^2}{\mathrm{d}\eta^2} - \alpha^2 \tag{3.5}$$

subjected to appropriate boundary conditions in (2.14). The integral operator L^{-1} can be formally represented by

$$f(\eta) = \mathrm{L}^{-1}\omega = \frac{1}{2\pi\mathrm{i}} \int_{c-\mathrm{i}\infty}^{c+\mathrm{i}\infty} \left(\frac{\int_0^\infty \mathrm{e}^{-s\eta'} \omega(\eta')\, \mathrm{d}\eta'}{s^2 - \alpha^2} \right) \mathrm{e}^{s\eta}\, \mathrm{d}s, \tag{3.6}$$

where Laplace transform and boundary conditions of f at $\eta = 0$ in (2.14) have been invoked. However, we shall invert L numerically by our spectral expansion.

It is easy to show that the eigenvalue problem (3.2) consists of two decoupled systems corresponding to the real and imaginary part of the complex eigenfunction $(\hat{u}, \hat{\omega}, \hat{\tau})$. In fact, the decoupled systems are related by the transformation

$$\begin{pmatrix} \mathrm{Re}\{\hat{u}\} \\ \mathrm{Im}\{\hat{\omega}\} \\ \mathrm{Re}\{\hat{\tau}\} \end{pmatrix} \rightarrow \begin{pmatrix} -\mathrm{Im}\{\hat{u}\} \\ \mathrm{Re}\{\hat{\omega}\} \\ -\mathrm{Im}\{\hat{\tau}\} \end{pmatrix}. \tag{3.7}$$

This explains why, for real eigenvalues, Haaland & Sparrow are able to consider only the modes

$$\left.\begin{aligned} \tilde{u} &= \hat{u}\cos\alpha\delta, \quad \tilde{\omega} = \hat{\omega}\sin\alpha\delta, \\ \tilde{\tau} &= \hat{\tau}\cos\alpha\delta, \quad \tilde{f} = \hat{f}\sin\alpha\delta. \end{aligned}\right\} \tag{3.8a}$$

There exists a conjugate eigenfunction set which is exactly $\frac{1}{2}\pi$ out of phase with (3.10a) in the spanwise direction but yields the same real eigenvalue,

$$\left.\begin{aligned} \tilde{u} &= -\hat{u}\sin\alpha\delta, \quad \tilde{\omega} = \hat{\omega}\cos\alpha\delta, \\ \tilde{\tau} &= -\hat{\tau}\sin\alpha\delta, \quad \tilde{f} = \hat{f}\cos\alpha\delta. \end{aligned}\right\} \tag{3.8b}$$

It should be noted that, for complex eigenvalues, the two conjugate eigenfunctions are distinct and Haaland & Sparrow's expansion of (3.8a) is incomplete. We shall compute the entire spectrum here.

We solve the semi-infinite-domain eigenvalue problem by a domain mapping technique coupled with a Chebyshev–Tau spectral expansion (Spalart 1984; Gottlieb & Orszag 1977; Ho & Chang 1988). We map the integral $\eta \in [0, \infty)$ into $\hat{\eta} \in (0, 1]$ by the exponential map

$$\hat{\eta} = \mathrm{e}^{-\eta}. \tag{3.9}$$

Spalart (1984) has observed that an expansion in terms of odd Chebyshev polynomials in $\hat{\eta}$ has the advantage of providing better resolution near the wall $\hat{\eta} = 1$ and coarser resolution away from the wall. We note that for the interval $\hat{\eta} \in (0, 1]$, both odd and even Chebyshev polynomials are complete but only the odd polynomials offer this preferential resolution near the wall. Moreover, odd polynomials satisfy all the requisite boundary conditions away from the wall at $\hat{\eta} = 0$. The boundary conditions at $\hat{\eta} = 1$ are not satisfied explicitly by the Chebyshev basis. To remedy this, we expand each variable in (3.2) with the appropriate number of extra expansion terms and use the unsatisfied boundary conditions to determine the extra degrees of freedom,

$$\hat{u} = \sum_{i=1}^{n+1} a_i P_i(\hat{\eta}), \quad \hat{\omega} = \sum_{i=1}^{n+2} b_i P_i(\hat{\eta}), \quad \hat{\tau} = \sum_{i=1}^{n+1} c_i P_i(\hat{\eta}), \tag{3.10a–c}$$

where $P_i(\hat{\eta})$ are the odd Chebyshev polynomials of degree $2i-1$. The deviation stream function $\hat{f}$ is likewise expanded and is related to the deviation vorticity (3.10b) by (2.13d). This is the Tau-spectral formulation for 'extra' boundary conditions (Canuto *et al.* 1988). We substitute (3.10) into (3.2) and take the inner product with only n bases to obtain a projected Jacobian

$$\boldsymbol{J}\boldsymbol{\phi} = \lambda\boldsymbol{\phi}, \tag{3.11a}$$

$$\boldsymbol{B}\boldsymbol{\phi} = 0, \tag{3.11b}$$

where $\boldsymbol{J}$ is a $(3n)\times(3n+4)$ rectangular matrix, $\boldsymbol{\phi}$ is a $(3n+4)$ vector, $\boldsymbol{\phi} = (\boldsymbol{a}, \boldsymbol{b}, \boldsymbol{c})^{\mathrm{t}}$, and $\boldsymbol{B}$ is a $4\times(3n+4)$ rectangular matrix representing the four boundary conditions at the wall in (2.14). In the evaluations of the inner products for $\boldsymbol{J}$, an orthogonal collocation technique (Villadsen & Stewart 1967) is used in which the derivatives are approximated by the analytical derivatives of the polynomial expansions of (3.10) which can be expressed in convenient recursive formulae. For example, the odd Chebyshev expansion of a function

$$\psi(\eta) = \sum_{i=1}^{n} a_i P_i(\hat{\eta}) \tag{3.12}$$

and its derivatives with respect to the untransformed coordinate η can now be expressed in terms of the odd Chebhshev polynomials in the transformed coordinate $\hat{\eta}$:

$$\frac{\mathrm{d}^m}{\mathrm{d}\eta^m}\psi(\eta) = \sum_{i=1}^{n} a_i^m P_i(\hat{\eta}), \tag{3.13}$$

then

$$a_i^1 = -(2i-1)\,a_i - 2\sum_{j=1+i}^{n}(2j-1)\,a_j, \tag{3.14a}$$

$$a_i^2 = (2i-1)^2 a_i + 4\sum_{j=1+i}^{n}(2j-1)\,(j-i)\,(j+i-1)\,a_j. \tag{3.14b}$$

(We have derived these formulae from the tables of Fox & Parker (1968) and Orszag (1971).) The inner products are then evaluated such that the residuals vanish exactly at the zeros of the odd Chebyshev polynomial $P_{n+3}(\hat{\eta})$ which are given by

$$\hat{\eta}_{n-k} = \cos\{(k+\tfrac{1}{2})\,\pi/(2n+5)\}, \quad k = 0, 1, 2, \ldots n-1. \tag{3.15}$$

In this manner, explicit integrations are not necessary and only evaluations of the odd Chebyshev polynomials at the zeros of (3.15) are required. Another major advantage of our spectral formulation is the fact that $\boldsymbol{B}$ in (3.11b) is independent of $\tilde{R}$, Pr and α and the rectangular matrix $\boldsymbol{J}$, which is the projection of the operator $\tilde{\mathbf{L}}$ in (3.3), only contains a submatrix, corresponding to the projection of L^{-1}, which has implicit dependence on α and must be evaluated for every α value. Other dependence on α, Pr and $\tilde{R}$ can be factored out explicitly, as is evident in (3.3), such that the submatrices need only be evaluated once. In contrast, a shooting method solution of the Orr–Sommerfeld equation in general requires duplicating the full numerical effort for each parameter value.

The projected eigenvalues of (3.11) can be easily obtained by expressing the last four elements of $\boldsymbol{\phi}$ in terms of the first $3n$ elements through (3.11b) and hence reducing (3.11a) to a $(3n)\times(3n)$ eigenvalue problem. A standard routine is used to evaluate the eigenvalues numerically. In figure 2, we depict the relative error

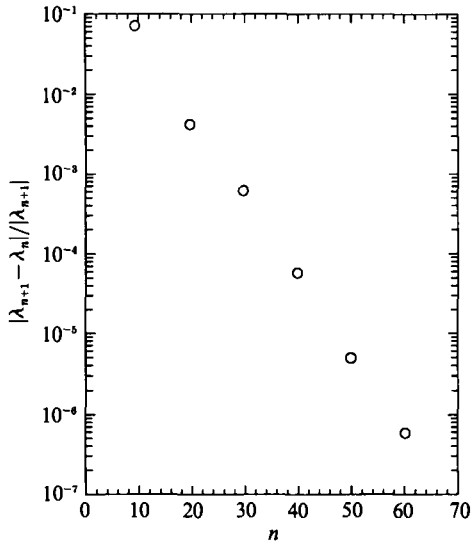

FIGURE 2. Convergence of the leading eigenvalue at $Pr = 5.5$, $\tilde{R} = 20$ and $\alpha = 0.8$ with respect to the mode number n.

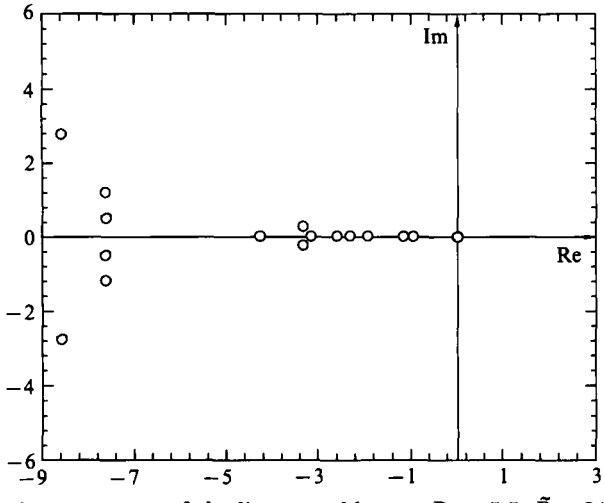

FIGURE 3. The eigenspectrum of the linear problem at $Pr = 5.5$, $\tilde{R} = 24.26$ and $\alpha = 1.292$.

$|\lambda_{n+1}-\lambda_n|/|\lambda_{n+1}|$ of the computed leading real eigenvalues as a function of mode number n for $\alpha = 0.8$, $\tilde{R} = 20$ and $Pr = 5.5$. As is evident, an exponential convergence with a moderate rate of decay (~ 0.23) is achieved, indicating that the spectral expansion is formulated correctly. In all subsequent computations, $n = 50$ is used and we estimate the error on the leading eigenvalue to occur at the fifth decimal place. A typical discrete normal spectrum for a given spanwise wavenumber is shown in figure 3 for $\alpha = \alpha_c = 1.292$, $\tilde{R} = 24.26$ and $Pr = 5.5$. Although some complex eigenvalues appear in the spectrum, the leading five eigenvalues are always real for realistic parameter values. Consequently, the 'exchange of stability' assumption by Haaland & Sparrow is correct even though the eigenvalue problem is not self-adjoint. Also, since the critical mode has a real eigenvalue, Eckhaus' sideband stability bound (1.1) applies. It will be shown later that downstream finite-amplitude rolls which retain the dimensional wavelength at criticality are stable to sideband disturbances.

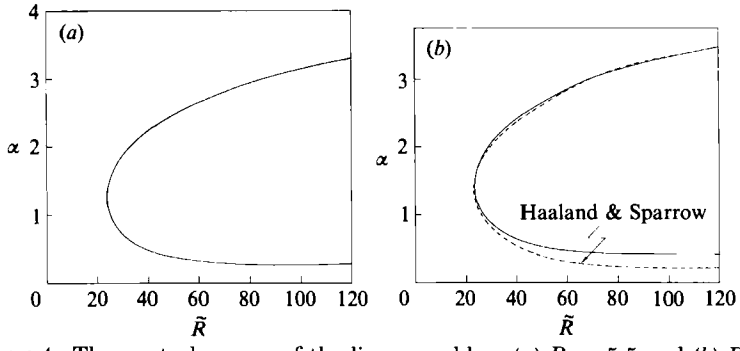

FIGURE 4. The neutral curves of the linear problem (*a*) $Pr = 5.5$ and (*b*) $Pr = 6.7$.

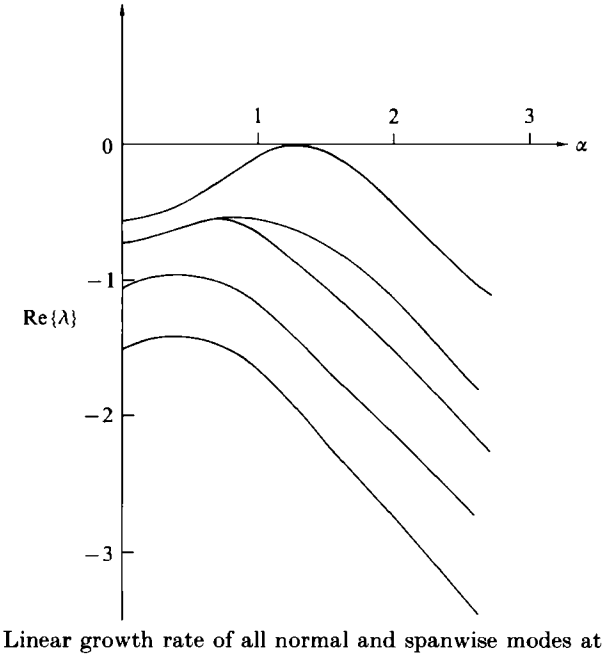

FIGURE 5. Linear growth rate of all normal and spanwise modes at onset for $Pr = 5.5$.

Pr	$\tilde{R}_c$	α_c
5.5	24.26	1.292
6.7	23.50	1.220

TABLE 1. Critical Reynolds number and wavenumbers for the main flow

This is consistent with the tracer streak photographs of Sparrow & Husar (1969) and Gilpin *et al.* (1978) which show very regular rolls before and after coalescence without any modulation. This then allows us to restrict our attention only to certain discrete modes (the superharmonics of $\frac{1}{2}\alpha$) and neglect the sidebands, even though a continuous band of wavenumber is linearly unstable. In figure 4, the neutral curves for $Pr = 5.5$ and 6.7 are shown and compared to the results of Haaland & Sparrow for $Pr = 6.7$. The computed critical Reynolds number and wavenumber, R_c and α_c, are tabulated in table 1. In figure 5, the full discrete normal spectrum for various cross-stream wavenumbers α is shown for $Pr = 5.5$ and $\tilde{R} = \tilde{R}_c$. The absence of

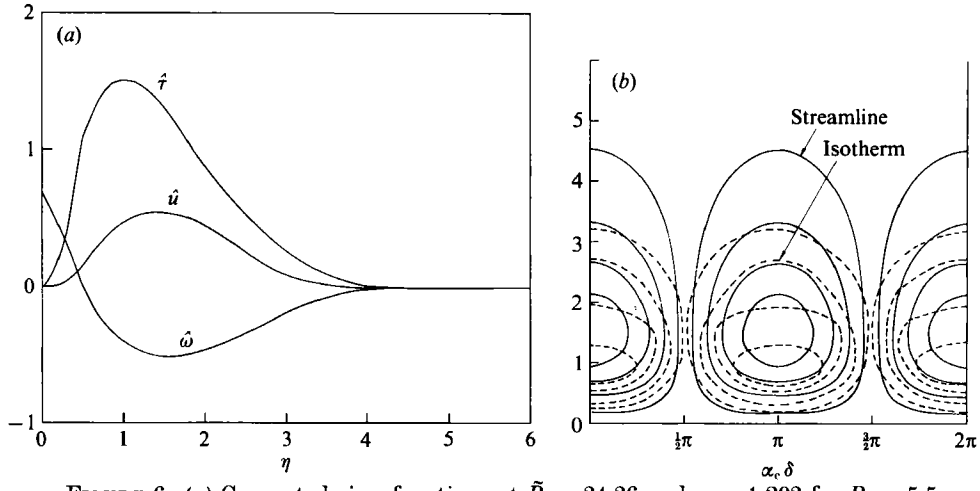

FIGURE 6. (*a*) Computed eigenfunctions at $\tilde{R}_c = 24.26$ and $\alpha_c = 1.292$ for $Pr = 5.5$. (*b*) Computed streamlines and isotherms for the critical condition of (*a*).

	a	*b*	*c*
1	−0.17603	−0.70109	0.95880
2	0.24468	0.92188	1.00000
3	−0.10447	−0.21442	0.48673
4	0.03726	−0.07077	0.66558
5	0.00841	0.12558	0.61442
6	−0.00152	−0.10150	0.60888
7	0.00516	0.06591	0.61764
8	−0.00494	−0.03843	0.59452
9	0.00492	0.02066	0.60170
10	0.00364	−0.01035	0.58115

TABLE 2. First ten spectral coefficients of the streamwise velocity, vorticity and temperature eigenvectors

'cross-over' indicates that the eigenvalue of the same normal spectral mode remains the most unstable one for all α values. In table 2, the first ten spectral coefficients of the eigenvectors $\boldsymbol{a}$, $\boldsymbol{b}$, and $\boldsymbol{c}$ of expansion (3.10) are tabulated for the leading normal mode at $\tilde{R} = \tilde{R}_c = 24.26$ and $\alpha = \alpha_c = 1.292$ in figure 5. The declining mode contribution further verifies the convergence of our spectral expansion and that sufficient modes have been taken. The maximum in the temperature eigenfunction $\hat{\tau}$ depicted with other critical eigenfunctions $\hat{u}$ and $\hat{\omega}$ in figure 6(*a*) is located slightly below the centre of this vortex. This longitudinal vortex roll is constructed in figure 6(*b*) from the critical velocity eigenfunction.

One distinct result of formulating (2.13) in the similarity variables is that the only explicit dependence on x is contained in $\tilde{R}$ which appears linearly in the equations. Consequently, the linear operator $\tilde{\mathbf{L}}$ of (3.3) can be conveniently decomposed into

$$\tilde{\mathbf{L}} = \tilde{\mathbf{L}}_0 + \alpha(\tilde{R} - \tilde{R}_c)\,\tilde{\mathbf{L}}_1, \tag{3.16}$$

where

$$\tilde{\mathbf{L}}_0 = \tilde{\mathbf{L}}(\tilde{R}_c). \tag{3.16b}$$

The operators $\tilde{\mathbf{L}}_0$ and $\tilde{\mathbf{L}}_1$ can be easily obtained from (3.3). It is important to note that (3.16*a*) is exact and not a local expansion near $\tilde{R}_c$. The eigenvalues of $\tilde{\mathbf{L}}$, however, do

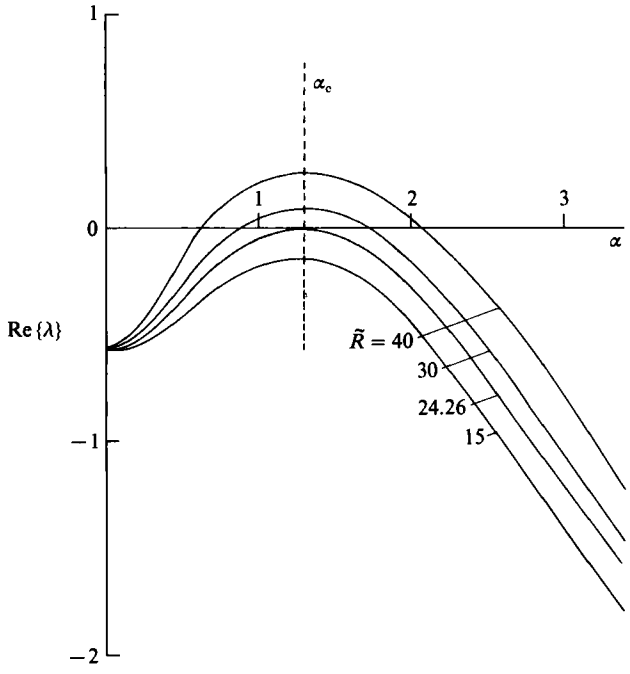

FIGURE 7. The linear growth rate of the most unstable normal mode for various Reynolds numbers. The growth rate varies linearly with respect to the Reynolds number.

not vary linearly with respect to $\tilde{R}$ except in the neighbourhood of $\tilde{R}_c$. Nevertheless, as seen in figure 7, our numerical result indicates that, for the conditions considered here, the maximum-growing wavenumber remains close to α_c. However, the dimensionless wavenumber α is obtained by scaling the actual wavelength by the boundary-layer thickness in (2.9). Hence, a constant α at every downstream position would actually imply a cross-stream roll wavelength that varies downstream. This is inconsistent with Sparrow & Husar's (1969) experimental observations. The actual wavelength selected downstream seems to remain at the same value at $\tilde{R}_c$. We shall abide by this observed wavelength selection mechanism and stipulate that the wavenumber chosen downstream is not the maximum-growing one α_c but

$$\alpha_* = \alpha_c(\tilde{R}/\tilde{R}_c)^{\frac{1}{3}} = \alpha_c(R/R_c)^{\frac{1}{3}}. \tag{3.17}$$

This path is depicted as a dashed curve in figure 8 within the neutral curve for $Pr = 5.5$. The other dashed curve in figure 8 represents the path of the fast-growing wavenumber at every downstream position. This fastest-growing wavenumber remains close to α_c. We note that path (3.17) implies that the subharmonic mode $\frac{1}{2}\alpha_*$ is more unstable than the $\frac{3}{2}$ mode $\frac{3}{2}\alpha_*$ since it shifts to the right of the fastest-growing mode, towards the right branch of the neutral curve. This will be shown to lead to the observed spanwise pairing whereas if the system is allowed to follow the fastest-growing path downstream, calculations indicate that the first secondary roll to appear would be one with wavenumber $\frac{3}{2}\alpha$. It should also be noted that both the path selecting the fastest-growing mode and the constant-wavelength path of (3.17) in figure 8 lie within the Eckhaus band of (1.1). One hence does not expect the monochromatic fundamental wave to be destabilized by sideband instability along both paths.

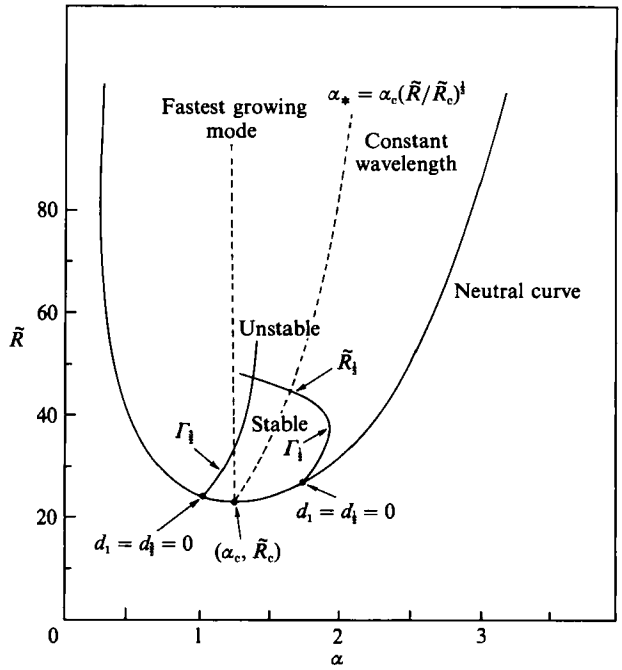

FIGURE 8. The neutral curve for $Pr = 5.5$ and other pertinent curves. The dashed lines represent the two possible wavelength selection mechanisms: (*a*) $\alpha_* = \alpha_c(\tilde{R}/\tilde{R}_c)^{\frac{1}{3}}$ (equation (3.17)) for constant dimensional wavelength and (*b*) the fastest growing wavelength. The two solid curves are subharmonic stability bounds $\Gamma_{\frac{1}{2}}$ and $\Gamma_{\frac{3}{2}}$ which are analogous to the Eckhaus bound for sideband instability. All monochromatic waves within the 'balloon' below these bounds are stable to $\frac{1}{2}$ and $\frac{3}{2}$ subharmonic disturbances. Intersections of the dashed lines with the subharmonic bounds represent the first onsets of subharmonic instability for the two paths.

m	a_0	a_1	a_2	a_3	a_4	a_5
$\frac{1}{2}$	-0.528	1.475×10^{-2}	1.744×10^{-3}	-2.669×10^{-4}	1.297×10^{-5}	-1.833×10^{-7}
1	0	3.184×10^{-2}	-4.601×10^{-4}	1.493×10^{-5}	-3.303×10^{-7}	3.101×10^{-9}
$\frac{3}{2}$	-0.320	1.254×10^{-2}	-1.154×10^{-4}	3.723×10^{-6}	-9.469×10^{-8}	9.978×10^{-10}
2	-0.957	-4.246×10^{-5}	-1.923×10^{-3}	1.434×10^{-4}	-4.173×10^{-6}	4.237×10^{-8}
$\frac{5}{2}$	-1.781	-5.31×10^{-2}	5.20×10^{-3}	-4.285×10^{-4}	1.456×10^{-5}	-1.698×10^{-7}
3	-2.713	-4.714×10^{-2}	-3.011×10^{-3}	1.496×10^{-4}	-1.217×10^{-6}	-2.352×10^{-8}

TABLE 3. Growth rates along path (3.17) in figure 8 ($Pr = 5.5$, $\tilde{R}_c = 24.26$) $d_m = \sum_{i=0}^{5} a_{i,m}(\tilde{R}-\tilde{R}_c)^i$

In the subsequent nonlinear analysis, we shall require the growth rates d of modes with wavenumbers α_*, $\frac{1}{2}\alpha_*$, $\frac{3}{2}\alpha_*$, $2\alpha_*$, $\frac{5}{2}\alpha_*$ and $3\alpha_*$ along path (3.17). These are computed from $\tilde{R} = \tilde{R}_c$ to $\tilde{R} \approx 80$ and fitted to a fifth-degree polynomial in $(\tilde{R}-\tilde{R}_c)$, with an error no more than 1%. The coefficients are listed in table 3. It is evident that growth rates do not vary linearly with respect to $(\tilde{R}-\tilde{R}_c)$ along path (3.17). Note also that the fundamental mode $m = 1$ is neutrally stable at $\tilde{R}_c$ but all the other modes have stable growth rates at $\tilde{R} = \tilde{R}_c$ since the expansion coefficients $a_{0,m}$ are negative for $m \neq 1$.

Finally, the dimensional versions of our computed cross-stream wavelength in table 1 for $Pr = 5.5$ are compared in table 4 to experimental values estimated from

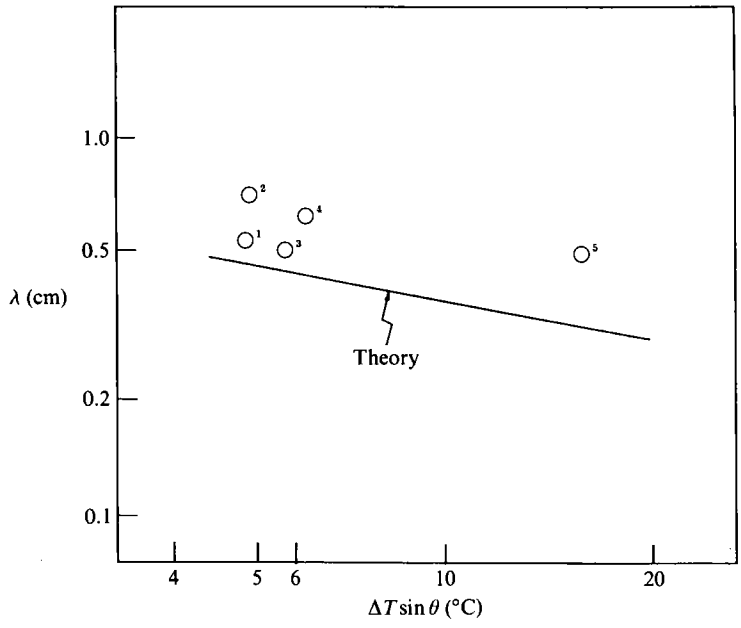

FIGURE 9. Variation of the spanwise wavelength of the primary roll with respect to $\Delta T \sin\theta$ from Sparrow & Husar's photograph for water, $Pr = 5.5$. The various data points are for $(\theta, \Delta T) = (25°, 12\ °C)$, $(35°, 9\ °C)$, $(20°, 17\ °C)$, $(35°, 11\ °C)$ and $(35°, 28\ °C)$ in numerical order.

θ (deg.)	$T_w - T_\infty$ (°C)	λ_{data} (cm)	λ_{theory} (cm)
35	11	0.61	0.424
25	12	0.53	0.456
20	17	0.50	0.436

TABLE 4. Comparison of predicted spanwise wavelength against the experimental data of Sparrow & Husar (1969) for $Pr = 5.5$ and $g\beta/\nu^2 = 5.808 \times 10^3\ \mathrm{K^{-1}\ cm^{-3}}$

the tracer streaks in the photographs from Sparrow & Husar's (1969) experiment with water. These photographs show very little downstream variation in the cross-stream wavelength beyond the onset of the longitudinal rolls until wavelength doubling occurs. These observed wavelengths are in satisfactory quantitative agreement with the computed values, as is evident in table 4. For $Pr = 5.5$, $\tilde{R}_c$ and α_c, which are only functions of Pr, are 24.26 and 1.292 respectively. Consequently, the dimensional wavelength λ, which can be conveniently expressed as

$$\lambda = \frac{2\pi}{\alpha_c}\left(\frac{\tilde{R}_c}{4}\right)^{\frac{1}{3}} (\tan\theta)^{-\frac{1}{3}} \kappa^{-\frac{4}{3}}, \tag{3.18}$$

has the following value for the case of water, with the fluid properties given in table 4:

$$\lambda = 0.783(\Delta T \sin\theta)^{\frac{1}{3}}. \tag{3.19}$$

This prediction is compared to our estimates of the observed wavelengths from Sparrow & Husar's photographs in figure 9. The good agreement is another verification of the validity of the modified parallel-flow approximation.

4. Secondary bifurcations beyond $\tilde{R}_c$

Equations (2.13) are invariant under the following two transformations

$$\delta \to \delta + \beta \quad \text{translation}, \tag{4.1a}$$

$$\begin{pmatrix} f \\ \omega \\ \delta \end{pmatrix} \to - \begin{pmatrix} f \\ \omega \\ \delta \end{pmatrix} \quad \text{reflection}. \tag{4.1b}$$

Transformation (4.1*a*) simply means that if a solution exists to (2.13), the same solution translated by an arbitrary distance β in the δ-direction is still a solution. This is expected of all solutions which bifurcate off the basic flow. Consequently, all secondary flows actually consist of a one-parameter family of solutions. This degeneracy is simply due to the arbitrariness of the origin of δ. The reflection symmetry (4.1*b*) corresponds physically to the two directions of flow of the vortices in figure 6(*b*). It is equivalent to a $\frac{1}{2}\pi$ phase shift in the δ-direction. Invariance with respect to those two transformations induce an $O(2)$ symmetry group. Proctor & Jones (1988) and Armbruster, Guckenheimer & Holmes (1988, 1989) have studied some generic bifurcations of systems with $O(2)$ symmetry. One ramification of this symmetry is that all eigenvalues of the basic state have 2-multiplicity, which has already been recognized in (3.7). We shall apply the invariant manifold technique of Roberts (1989), which is an extension of the centre-unstable manifold techniques, in the next section to obtain analytical estimates to the new solutions and determine their stability for the present problem. Specifically, we shall scrutinize subharmonic instability which will be shown to precede some of the superharmonic instabilities revealed by Armbruster *et al.*

Considering only the discrete modes of the main flow that are superharmonics of $\frac{1}{2}\alpha_*$, which is equivalent to imposing a periodic boundary condition in the δ-direction of period $4\pi/\alpha_*$, we expand $\tilde{u}$, ω and $\tilde{\tau}$ in (2.13) in terms of the eigenfunctions of (3.2) which satisfy this periodicity condition,

$$\begin{pmatrix} \tilde{u} \\ \omega \\ \tilde{\tau} \end{pmatrix} = \sum_{\substack{m=-\infty \\ m \neq 0}}^{\infty} A_{m/2}(t) \begin{pmatrix} \hat{u}_{m/2}(\eta) \\ \hat{\omega}_{m/2}(\eta) \\ \hat{\tau}_{m/2}(\eta) \end{pmatrix} \exp(\mathrm{i}m\alpha_* \delta/2), \tag{4.2}$$

where $A_{m/2}$ is the complex mode coefficient, and since the expanded variables are real

$$A_{-m/2} = A^*_{m/2}, \tag{4.3}$$

where * denotes complex conjugate. Since there is no crossing of the normal modes as shown in figure 5, all the spanwise discrete modes of (4.2) correspond to the leading normal mode. We hence omit intermode interaction between the normal modes. It should be pointed out that path (3.17) lies within the Eckhaus bound (1.1). Consequently, the primary roll solution with wavenumber α_* is stable to sideband instability. This is consistent with the lack of roll modulation in the experiments. Consequently, the subharmonic instability of the primary roll can be studied with the discrete Fourier expansion in (4.2) instead of a continuous one. We have also neglected the $m = 0$ mode in (4.2). In essence, this is an omission of interaction between the disturbances and the mean flow. We show in the Appendix that this mean flow interaction does not affect our prediction of subharmonic instability to leading order.

The eigenfunction $(\hat{u}_{m/2}, \hat{\omega}_{m/2}, \hat{\tau}_{m/2})^{\mathrm{t}}$ is the leading one of (3.2) at $\alpha = \frac{1}{2}m\alpha_*$. From (3.7) and (3.8), (4.2) can also be written as

$$\begin{pmatrix} \tilde{u} \\ \omega \\ \tilde{\tau} \end{pmatrix} = \sum_{m=1}^{\infty} \mathrm{Re}\{A_{m/2}(t)\} \begin{pmatrix} \hat{u}_{m/2} \cos(\mathrm{i}m\alpha_* \delta/2) \\ \hat{\omega}_{m/2} \sin(\mathrm{i}m\alpha_* \delta/2) \\ \hat{\tau}_{m/2} \cos(\mathrm{i}m\alpha_* \delta/2) \end{pmatrix} + \sum_{m=1}^{\infty} \mathrm{Im}\{A_{m/2}(t)\} \begin{pmatrix} -\hat{u}_{m/2} \sin(\mathrm{i}m\alpha_* \delta/2) \\ \hat{\omega}_{m/2} \cos(\mathrm{i}m\alpha_* \delta/2) \\ -\hat{\tau}_{m/2} \sin(\mathrm{i}m\alpha_* \delta/2) \end{pmatrix}, \tag{4.4}$$

which is more convenient for computational purposes.

Equation (2.13) can be formally written as

$$\frac{\partial}{\partial t} \begin{pmatrix} \tilde{u} \\ \omega \\ \tilde{\tau} \end{pmatrix} = \mathbf{L}_0 \begin{pmatrix} \tilde{u} \\ \omega \\ \tilde{\tau} \end{pmatrix} + (\tilde{R} - \tilde{R}_{\mathrm{c}}) \mathbf{L}_1 \begin{pmatrix} \tilde{u} \\ \omega \\ \tilde{\tau} \end{pmatrix} + \frac{\tilde{R}}{\tan\theta} N(\tilde{u}, \omega, \tilde{\tau}) \tag{4.5}$$

where $\mathbf{L}_0 = \mathbf{L}(\tilde{R}_{\mathrm{c}})$ and $\mathbf{L}$, $\mathbf{L}_0$ and $\mathbf{L}_1$ correspond to $\tilde{\mathbf{L}}$, $\tilde{\mathbf{L}}_0$ and $\tilde{\mathbf{L}}_1$ of (3.3) and (3.16) and N denotes the quadratic nonlinear terms. Substituting (4.2) or (4.4) into (4.5) and taking the inner product

$$\langle \boldsymbol{u}, \boldsymbol{v} \rangle = \frac{\alpha_*}{\pi} \int_0^{\infty} \int_0^{4\pi/\alpha_*} \boldsymbol{u} \cdot \boldsymbol{v} \, \mathrm{d}\delta \, \mathrm{d}\eta \tag{4.6}$$

one obtains the amplitude equation

$$\frac{\mathrm{d}A_{m/2}}{\mathrm{d}t} = d_{m/2} A_{m/2} + R(R/R_{\mathrm{c}})^{\frac{1}{3}} \sum_{\substack{n=-\infty \\ n \neq 0}}^{\infty} P[n/2, (m-n)/2] A_{n/2} A_{(m-n)/2}, \tag{4.7}$$

where $d_{m/2}$ is simply the growth rate of the $\frac{1}{2}m$ mode along the path (3.17) as given in table 3. We have also replaced $\tilde{R}/\tan\theta$ by R from (2.12) in the multiplying factor to the nonlinear term. Since every nonlinearity in (2.13) contains a first derivative in δ and no other δ derivatives, a factor of $(R/R_{\mathrm{c}})^{\frac{1}{3}}$ appears in the projected form of (4.7) in addition to the original R factor. Explicit dependence on θ does not appear, although θ is implicitly contained in $R_{\mathrm{c}} = \tilde{R}_{\mathrm{c}}/\tan\theta$. Dependence on Pr, however, is extremely complex since the basic state of (2.2), which must be computed numerically, is dependent on Pr. In table 5, the 24 interaction coefficients $P[\frac{1}{2}k, \frac{1}{2}]$ corresponding to a 6-mode truncation of (4.7) are tabulated: These coefficients are only dependent on Pr, which is fixed at 5.5. The symmetries of (4.1) are also retained in the amplitude equations where translation symmetry (4.1a) corresponds to a rotation in the phase of the amplitude

$$A_{m/2} \rightarrow A_{m/2} \exp(\mathrm{i}m\beta\alpha_{\mathrm{c}}/2) \tag{4.8a}$$

and reflection symmetry (4.1b) corresponds to symmetry of (4.7) with respect to complex conjugation

$$A_{m/2} \rightarrow A^*_{m/2} \tag{4.8b}$$

which is evident from the symmetry of table 5.

It should be noted that (4.7) is an exact amplitude expansion of (2.13). Although the eigenfunctions at criticality are used for the Galerkin-type expansion, the

k \ l	$\frac{1}{2}$	$-\frac{1}{2}$	1	-1	$\frac{3}{2}$	$-\frac{3}{2}$	2	-2	$\frac{5}{2}$	$-\frac{5}{2}$	3	-3
$\frac{1}{2}$	0.019	0	−3.08	0	−1.75	0	−4.02	0	−4.88	0	0	0
$-\frac{1}{2}$	0	0	0.161	0	1.17	0	4.83	0	3.62	0	4.78	0
1	−3.08	0.161	−15.5	0	−10.3	0	−18.04	0	0	0	0	0
−1	0	0	0	0	11.5	0	7.46	0	19.1	0	14.1	0
$\frac{3}{2}$	−1.75	1.17	−10.3	11.5	−5.62	0	0	0	0	0	0	0
$-\frac{3}{2}$	0	0	0	0	0	0	10.92	0	26.2	0	7.11	0
2	−4.02	4.83	−18.4	7.46	0	10.92	0	0	0	0	0	0
−2	0	0	0	0	0	0	0	0	16.4	0	2.66	0
$\frac{5}{2}$	−4.88	3.62	0	19.1	0	2.62	0	16.4	0	0	0	0
$-\frac{5}{2}$	0	0	0	0	0	0	0	0	0	0	13.4	0
3	0	4.78	0	14.1	0	7.11	0	2.66	0	13.4	0	0
−3	0	0	0	0	0	0	0	0	0	0	0	0

TABLE 5. Nonlinear interaction coefficients ($\times 10^{-2}$) for $Pr = 5.5$

amplitude equations are not restricted to near critical conditions as in many classical Stuart–Landau derivations. This is because the growth rate in our problem is not a local linear expansion near $\tilde{R}_c$ and the factor $R(R/R_c)^{\frac{1}{3}}$ premultiplying the nonlinear terms is not evaluated at $R = R_c = \tilde{R}_c/\tan\theta$. However, in addition to solving (4.7) numerically, we shall also simplify its analysis in the next section by using invariant and centre-unstable manifold techniques near certain critical points (Guckenheimer & Holmes 1983; Carr 1981; Armbruster *et al.* 1989; Roberts 1989). These techniques allow us to obtain analytical results regarding the secondary evolution of the rolls for $\tilde{R}$ beyond $\tilde{R}_c$ that are difficult to decipher from a direct numerical solution of (4.7). After these techniques are applied, near-critical amplitude equations similar to the classical ones are then obtained. However, unlike classical theories, secondary bifurcations such as the subharmonic instability of the primary roll solution can also be analysed.

We shall first construct the solutions to (4.7) numerically. To this end, we use the Cartesian coordinate transform

$$A_l = x_l + iy_l \tag{4.9}$$

and derive from (4.7) twice the number of equations for the real variables x_l and y_l. For $Pr = 5.5$ and for the range of $\tilde{R}$ values where at most the 1, $\frac{1}{2}$ and $\frac{3}{2}$ modes are unstable, we have found by numerical solution of (4.7) with various truncations of n that a 6-mode model (or a 12-mode model in the Cartesian coordinate of (4.9)) is sufficient to ensure accuracy in $|A_1|$ to the third decimal place in the regions of interest. We use a continuation scheme for the solution which is similar to our earlier solution of the Kuramoto–Sivashinsky equation (Chen & Chang 1986). In many cases, it is more convenient to express the amplitudes in polar coordinates

$$A_l = r_l(t)\,e^{i\theta_l(t)}. \tag{4.10}$$

In both coordinates, a finite-amplitude standing roll is represented by a fixed point in (x_l, y_l) or (r_l, θ_l). Travelling rolls which propagate in the cross-stream direction z are represented by a limit-cycle in the multi-dimensional Cartesian coordinate (x_l, y_l) but by constant amplitudes r_l and phases θ_l which vary linearly in time in the polar coordinate.

The primary roll solution with only superharmonic modes (1, 2, 3) is shown in figure 10 for $\theta = 20°$. The general unfolding of superharmonic solutions to amplitude equations of systems with $O(2)$ symmetry have been studied by Armbruster *et al.* (1988) and Proctor & Jones (1988). As is consistent with their prediction, a finite-amplitude roll solution bifurcates supercritically from $\tilde{R}_c = R_c \tan 20° = 24.26$. As evident from the amplitudes listed in table 6, this primary roll solution contains mostly the fundamental and the overtone with negligible contribution from the higher superharmonic and zero contribution from the subharmonics. It retains the same cross-stream wavelength as at criticality for all values of $\tilde{R}$ and spans from $\tilde{R}_c$ to approximately $\tilde{R} = 200$ where the first overtone-$2\alpha_*$ destabilizes. However, before this first overtone dominates such that a splitting of rolls occurs, Armbruster *et al.* (1988) have shown by a centre-unstable manifold theory that the primary roll will be destabilized by a travelling wave instability involving only the fundamental α_* and the overtone-$2\alpha_*$. The ensuing travelling roll solution will eventually yield wave packets (travelling waves) and even heteroclinic bifurcations which have been linked to intermittent bursts in boundary layers (Armbruster *et al.* 1988; Aubry *et al.* 1988). For the present problem, this travelling wave instability of the primary roll actually propagates in the cross-stream direction. Such a transverse wave instability of the

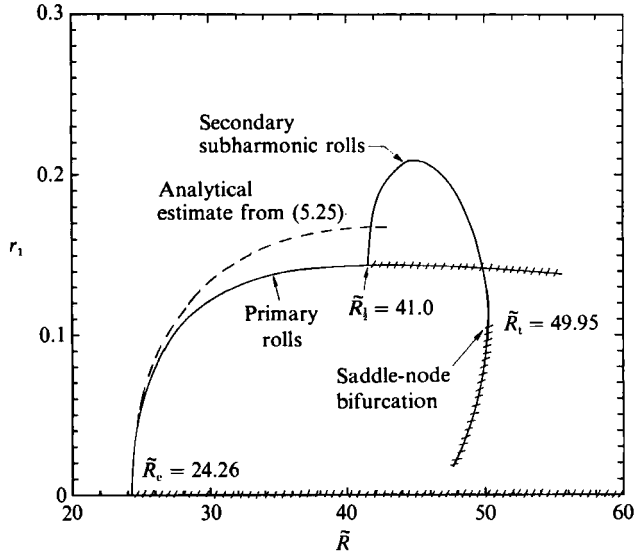

FIGURE 10. Bifurcation diagram for the amplitude of the fundamental mode as a function of $\tilde{R}$ along the constant wavelength path of figure 8 for $Pr = 5.5$ and $\theta = 20°$. The subharmonic roll first appears at $\tilde{R}_{\frac{1}{2}} = 41.0$ but is annihilated at $\tilde{R}_t = 49.95$ via a saddle-node bifurcation. Solid branches denote stable solutions and hatched ones denote unstable solutions.

$\tilde{R}$	r_1	r_2	r_2/r_1	r_3	$r_{\frac{1}{2}}$	$r_{\frac{3}{2}}$	$r_{\frac{5}{2}}$
Primary							
24.35	0.0021	0.002	0.095	0.000			
30	0.1206	0.0685	0.568	0.0170			
35	0.1378	0.0959	0.696	0.0297			
41 ($\tilde{R}_{\frac{1}{2}}$)	0.1431	0.1125	0.786	0.0392			
45	0.1431	0.1189	0.831	0.0431			
50	0.1413	0.1240	0.878	0.0465			
55	0.1386	0.1272	0.918	0.04903			
Secondary subharmonic roll							
42	0.1815	0.1216	0.670	0.0553	0.622	0.0587	0.0062
44	0.2069	0.1316	0.636	0.0736	1.102	0.0589	0.0116
46	0.2057	0.1246	0.6057	0.0759	1.1204	0.0412	0.0174
49.95 ($\tilde{R}_t$)	0.1281	0.0660	0.5152	0.0392	1.1005	0.0266	0.0256

TABLE 6. Numerical solutions of the amplitude equations ($Pr = 5.5$ and $\theta = 20°$). Phase differences $\phi_1 = 2\theta_1 - \theta_2$ and $\phi_3 = \theta_1 + \theta_2 - \theta_3$ are $-\pi$; $\phi_2 = 2\theta_{\frac{3}{2}} - \theta_1 - \theta_2$ is 0, $\phi_4 = \theta_2 - \theta_{\frac{3}{2}} - \theta_{\frac{1}{2}}$ is π and $\phi_5 = \theta_3 - \theta_{\frac{5}{2}} - \theta_{\frac{1}{2}}$ is 2π.

rolls has never been observed experimentally although downstream travelling waves are generated from rolls in a Couette flow when heated sufficiently from below (Clever *et al.* 1977). We show subsequently, both numerically in this section and analytically in the next, that for the present problem the primary roll is first destabilized by a subharmonic instability which precedes the travelling wave instability. This is, of course, consistent with experimental observations.

To study subharmonic instability of the finite-amplitude vortices, we insert the subharmonic modes $\frac{1}{2}$, $\frac{3}{2}$ and $\frac{5}{2}$ of the basic flow in (4.7). As shown in figure 10, the finite-amplitude primary roll destabilizes to subharmonic instability at $\tilde{R} = \tilde{R}_{\frac{1}{2}} =$

41.0. (Note that this $\tilde{R}_{\frac{1}{2}}$ corresponds to a subharmonic instability of the primary roll solution and not the subharmonic instability of the basic flow where $d_{\frac{1}{2}}$ vanishes. In fact, bifurcation of a pure subharmonic mode from the basic flow does not exist.) As shown in figure 10 and table 6, a finite-amplitude subharmonic roll emanates from the primary roll at this bifurcation point. This subharmonic roll still receives some non-zero contribution from the fundamental mode (r_1 in table 6) but it is dominated by the subharmonic mode ($r_{\frac{1}{2}}$ in table 6). In figure 10, only the r_1 component of the subharmonic roll solution is depicted. The $r_{\frac{1}{2}}$ component increases monotonically in the immediate neighbourhood beyond $\tilde{R}_{\frac{1}{2}}$ as shown in table 6. The travelling wave instability of Armbruster *et al.* (1988) was not observed prior to $\tilde{R}_{\frac{1}{2}}$ where the subharmonic instability first appears. Moreover, as is evident from figure 8 and table 6, even though the $\frac{3}{2}$ mode is nearly unstable (with its growth rate at $\tilde{R}_{\frac{1}{2}}$ equal to -0.08), the secondary subharmonic roll which represents the merged rolls has a negligible $\frac{3}{2}$-mode content. Hence, this subharmonic destabilization of the primary roll is due mainly to the $\frac{1}{2}$ mode and the $\frac{3}{2}$ mode is not excited in the nonlinear interaction. This is quite distinct from the mechanism in free shear layers where Kelly (1967) has predicted the excitation of the $\frac{3}{2}$ mode. The contribution of the $\frac{3}{2}$ mode will be scrutinized in the next section.

The phase shift between the 1 mode and the $\frac{1}{2}$ mode near the secondary bifurcation point $\tilde{R}_{\frac{1}{2}}$ is determined by

$$\theta_1 - 2\theta_{\frac{1}{2}} = \phi_1 + \phi_2 + 2\phi_4, \tag{4.11}$$

where the phase differences ϕ_i are defined and tabulated in table 6. Along the new secondary roll, table 6 indicates that ϕ_1 is equal to $-\pi$, ϕ_2 is zero, and ϕ_4 is π. Consequently, the dominant $\frac{1}{2}$ mode is shifted relative to the 1 mode by half of the wavelength of the 1 mode such that the maxima (minima) of the $\frac{1}{2}$ mode is asymmetrically located at $\frac{1}{4}$ ($\frac{1}{2}\pi$ phase) and $\frac{3}{4}$ ($\frac{3}{2}\pi$ phase) the fundamental wavelength from the maxima (minima) of the 1 mode. Since the maxima and minima of the modes correspond to the upward- and downward-flowing sides of the roll in figure 6(*b*), this means that the sides are likewise spatially dislocated after the rolls merged. This is consistent with the dislocation of the tracer streak, which resides in the upward-flowing side as clearly shown by the photographs of Sparrow & Husar (1969), in the schematic of figure 1. This phase shift will be scrutinized in more detail in the next section. The secondary subharmonic roll solution with a large $\frac{1}{2}$ mode content does not persist indefinitely, however. It quickly undergoes a saddle-node (turning point) bifurcation at $\tilde{R}_t = 49.95$. This saddle-node bifurcation results from a complex nonlinear interaction among the fundamental, overtone and the $\frac{1}{2}$ subharmonic modes of the basic flow along path (3.17). As shown in table 6, all three modes contribute non-negligibly to the secondary subharmonic roll near $\tilde{R}_t$. Although the linear growth rates of both the fundamental and $\frac{1}{2}$ subharmonic modes of the basic flow continue to increase downstream beyond $\tilde{R}_t$ on path (3.17), their nonlinear interaction has eliminated the secondary subharmonic roll entirely. The subharmonic component $r_{\frac{1}{2}}$ of this solution actually decreases slightly near $\tilde{R}_t$ in spite of the increasing linear growth rate. The possibility of eliminating a finite-amplitude roll through a saddle-node bifurcation is quite surprising although it is consistent with the experimental observations of Sparrow & Husar (1969) and Haaland & Sparrow (1973). The physical mechanism behind this dramatic nonlinear phenomenon remains to be studied. Beyond $\tilde{R}_t$, the primary roll still exists but it remains unstable to subharmonic disturbances as shown in figure 10. Consequently, stable rolls do not exist beyond $\tilde{R}_t$. Our numerical integration of the initial-value problem shows irregular but bounded trajectories at $\tilde{R} = 52.0$ as shown in figure 11. This implies

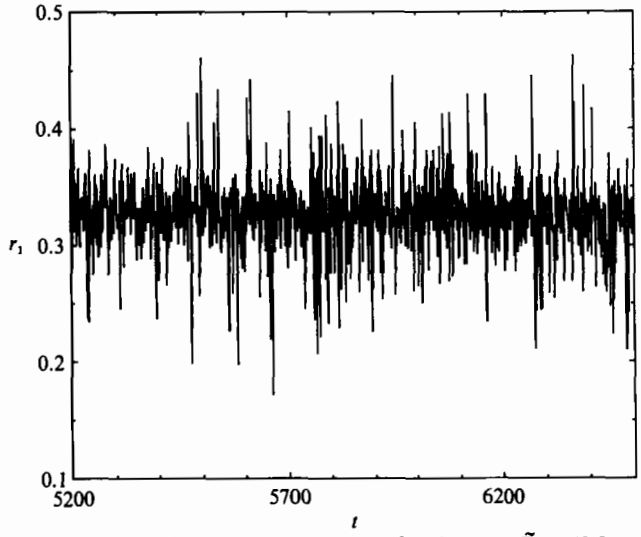

FIGURE 11. The irregular temporal behaviour at $\tilde{R} = 52$ beyond $\tilde{R}_t$.

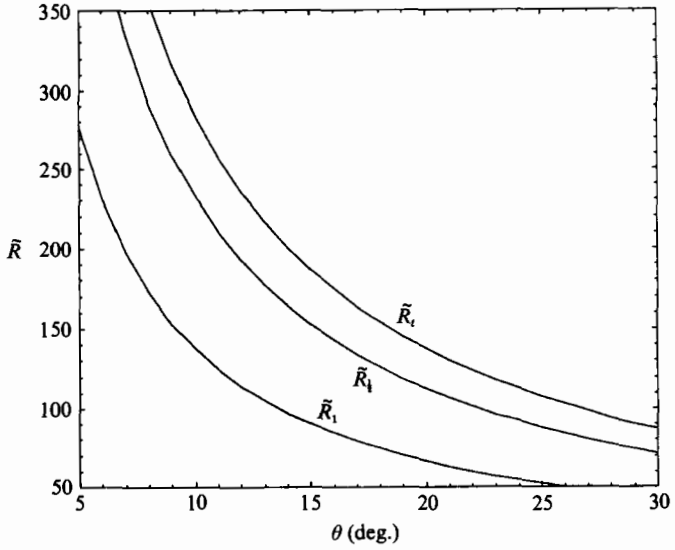

FIGURE 12. The dependence of the various critical Reynolds numbers as functions of inclination angle θ for $Pr = 5.5$. The path chosen is the constant dimensional-wavelength dashed curved in figure 8.

that the merged rolls are quickly annihilated by irregular fluctuations. Even this prediction is consistent with the experiments of Sparrow & Husar (1969) and Haaland & Sparrow (1973). For an inclination angle of 35° ($Pr = 5.5$, $T_w - T_\infty = 11$ °C and $g\beta/\nu^2 = 5.808 \times 10^3$ k^{-1} cm^{-3}), estimates from their tracer streak photographs indicate that $R_{\frac{1}{2}}/R_1 = 2.8$ and $R_t/R_{\frac{1}{2}} = 1.3$. In contrast, our predicted values are $R_{\frac{1}{2}}/R_1 = 1.7$ and $R_t/R_{\frac{1}{2}} = 1.2$. Interestingly, the data of Gilpin *et al.* (1978) for a heated Blasius layer ($U_\infty = 7.6$ cm/s, $\Delta T = 5.1 \times 10^{-4}$) also show a rapid dissipation after the rolls merge. Their transition points yield $R_{\frac{1}{2}}/R_1 = 1.7$ and $R_t/R_{\frac{1}{2}} = 1.7$. This suggests that very similar mechanisms occur for the two systems. Finally, we depict the computed critical Reynolds numbers for various inclination angles θ in figure 12 for $Pr = 5.5$.

We have also carried out a global analysis within the neutral curve of figure 8, instead of restricting ourselves only to path (3.17). For this effort, we have computed the growth rates of all modes $d_m(\tilde{R}, \alpha)$ within the region depicted in figure 8. A fifth-order expansion in both $(\alpha-\alpha_c)$ and $(\tilde{R}-\tilde{R}_c)$ is then carried out, analogous to the single-parameter expansion in table 3 along path (3.17). The nonlinear coefficients $P[n, m]$ of (4.7) are only dependent on Pr and hence are path independent within the neutral curve. We then proceed along a family of constant-α paths, beginning at the neutral curve. Along each path, we numerically construct the primary roll solution from (4.7) and analyse its stability. For all paths taken, the primary roll is either first destabilized by the $\frac{1}{2}$ subharmonic or the $\frac{3}{2}$ subharmonic. The dominant subharmonic is discerned from the eigenvector at the onset of subharmonic instability. The $\frac{1}{2}$ mode is dominant for primary rolls near the right neutral curve and the $\frac{3}{2}$ mode is dominant for those near the left neutral curve. The two computed subharmonic stability bounds $\Gamma_{\frac{1}{2}}$ and $\Gamma_{\frac{3}{2}}$ for all primary rolls within the neutral curve are depicted as solid curves in figure 8. The 'balloon' region bounded above by these two curves contains primary rolls stable to both $\frac{1}{2}$ and $\frac{3}{2}$ subharmonic disturbances. The point $\tilde{R}_{\frac{1}{2}}$ computed from path (3.17) lies at the intersection of this path with $\Gamma_{\frac{1}{2}}$. The bound $\Gamma_{\frac{1}{2}}$ for instability to the $\frac{1}{2}$ subharmonic emanates from a resonant point on the right neutral curve $(\tilde{R}, \alpha)$ with both α and $\frac{1}{2}\alpha$ are neutrally stable, namely at the given $\tilde{R}$, α lies on the right neutral curve and $\frac{1}{2}\alpha$ lies on the left neutral curve. The $\Gamma_{\frac{3}{2}}$ bound emanates from another resonant point $(\tilde{R}, \alpha)$ on the left neutral curve where α is neutrally stable and $\frac{3}{2}\alpha$ is also neutrally stable on the right neutral curve.

5. Analytical construction

Some of the computed results in the previous section using six complex amplitude equations can be estimated with a local centre manifold or centre-unstable manifold analysis near the bifurcation points. There are several advantages to such an analytical construction other than verification of our numerical values. The resulting amplitude equations are lower in dimension and are far simpler to analyse than the high-dimensional systems of the previous section. The classical nonlinear theories, such as those developed by Kelly (1967), Janssen (1986) and Monkewitz (1988), also yield low-order amplitude equations involving only the unstable and neutral modes. Consequently, the analysis provides a new derivation of the classical equations without using the usual multi-scale techniques. Carr & Muncaster (1983), for example, have employed the centre manifold theory to derive the Stuart–Landau amplitude equations near the critical point where only the fundamental mode is dominant. We shall use extensions of this theory, the centre-unstable and invariant manifold theories, to obtain amplitude equations near second bifurcation points where multiple dominant modes appear, such as at $\tilde{R}_{\frac{1}{2}}$ where the fundamental, $\frac{1}{2}$ and $\frac{3}{2}$ modes are all dominant. The travelling wave instability of Armbruster *et al.* also occurs when the fundamental and the first overtone are both dominant. Like the Stuart–Landau equation, these low-order amplitude equations allow us to scrutinize the key nonlinear interactions that govern some distinct qualitative features of the transitions. Such features include direction of bifurcation, stability of bifurcated solutions and the observed shift after coalescence. Since our amplitude equations are general to any system with quadratic nonlinearity and $O(2)$ symmetry, the identification of the key nonlinear coefficients is extremely useful. It allows us to predict some behaviour of a given system without resorting to the brute-force numerical integration of the previous section. Merely the key nonlinear coefficients

need to be evaluated. We shall verify these predictions from low-order amplitude equations to the exact numerical results of the previous section. We also use the centre-unstable manifold theory to justify our omission of mean flow interaction in the Appendix.

The six-dimensional version of (4.7) is

$$\frac{\mathrm{d}A_{\frac{1}{2}}}{\mathrm{d}t} = d_{\frac{1}{2}}A_{\frac{1}{2}} + \hat{R}\{P[1,-\tfrac{1}{2}]A_1A_{\frac{1}{2}}^* + P[\tfrac{3}{2},-1]A_{\frac{3}{2}}A_1^* + P[2,-\tfrac{3}{2}]A_2A_{\frac{3}{2}}^* + P[\tfrac{5}{2},-2]A_{\frac{5}{2}}A_2^* + P[3,-\tfrac{5}{2}]A_3A_{\frac{5}{2}}^*\}, \quad (5.1a)$$

$$\frac{\mathrm{d}A_1}{\mathrm{d}t} = d_1A_1 + \hat{R}\{P[\tfrac{1}{2},\tfrac{1}{2}]A_{\frac{1}{2}}^2 + P[2,-1]A_2A_1^* + P[3,-2]A_3A_2^* + P[\tfrac{3}{2},-\tfrac{1}{2}]A_{\frac{3}{2}}A_{\frac{1}{2}}^* + P[\tfrac{5}{2},-\tfrac{3}{2}]A_{\frac{5}{2}}A_{\frac{3}{2}}^*\}, \quad (5.1b)$$

$$\frac{\mathrm{d}A_{\frac{3}{2}}}{\mathrm{d}t} = d_{\frac{3}{2}}A_{\frac{3}{2}} + \hat{R}\{P[1,\tfrac{1}{2}]A_{\frac{1}{2}}A_1 + P[2,-\tfrac{1}{2}]A_2A_{\frac{1}{2}}^* + P[\tfrac{5}{2},-1]A_{\frac{5}{2}}A_1^* + P[3,-\tfrac{3}{2}]A_3A_{\frac{3}{2}}^*\}, \quad (5.1c)$$

$$\frac{\mathrm{d}A_2}{\mathrm{d}t} = d_2A_2 + \hat{R}\{P[1,1]A_1^2 + P[3,-1]A_3A_1^* + P[\tfrac{5}{2},-\tfrac{1}{2}]A_{\frac{5}{2}}A_{\frac{1}{2}}^* + P[\tfrac{3}{2},\tfrac{1}{2}]A_{\frac{3}{2}}A_{\frac{1}{2}}\}, \quad (5.1d)$$

$$\frac{\mathrm{d}A_{\frac{5}{2}}}{\mathrm{d}t} = d_{\frac{5}{2}}A_{\frac{5}{2}} + \hat{R}\{P[2,\tfrac{1}{2}]A_2A_{\frac{1}{2}} + P[3,-\tfrac{1}{2}]A_3A_{\frac{1}{2}}^* + P[1,\tfrac{3}{2}]A_1A_{\frac{3}{2}}\}, \quad (5.1e)$$

$$\frac{\mathrm{d}A_3}{\mathrm{d}t} = d_3A_3 + \hat{R}\{P[1,2]A_1A_2 + P[\tfrac{3}{2},\tfrac{3}{2}]A_{\frac{3}{2}}^2 + P[\tfrac{1}{2},\tfrac{5}{2}]A_{\frac{1}{2}}A_{\frac{5}{2}}\}, \quad (5.1f)$$

where
$$\hat{R} = R(R/R_c)^{\frac{1}{3}} = \tilde{R}(\tilde{R}/\tilde{R}_c)^{\frac{1}{3}}/\tan\theta \quad (5.1g)$$

and the growth rates are evaluated along path (3.17),

$$d_m = d_m(\tilde{R}, \alpha_*(\tilde{R})).$$

Along path (3.17), these six modes destabilize in the order of modes, 1, $\frac{1}{2}$, $\frac{3}{2}$, 2, $\frac{5}{2}$ and 3. In fact, modes $\frac{5}{2}$ and 3 are always stable in the region of interest. In the general theory of centre-unstable manifold projection (Armbruster *et al.* 1989), the dynamics of the dominant unstable and nearly neutral modes is deciphered by expressing the stable modes in terms of these modes. Upon substituting such centre and unstable manifold expansions into the dominant unstable and nearly neutral modes, one will then have reduced the system equations to a far smaller number of amplitude equations.

As an example, we begin by deriving the Stuart–Landau equation near $\tilde{R}_c$. Near this bifurcation point, the only nearly neutral mode is the fundamental mode. Because the amplitude A_1 is complex, (5.1) indicates that there are two zero eigenvalues at $\tilde{R}_c$, which is a manifestation of the $O(2)$ symmetry. We seek the direction and amplitude of the finite-amplitude roll near $\tilde{R}_c$ along path (3.17) which is the usual information offered by the Stuart–Landau equation. Since the convective nonlinearity in (2.13) and its counterpart in the amplitude equations (5.1) are quadratic, the nonlinear 'saturation' of the linear growth cannot be due to interaction of the unstable fundamental mode ($m = 1$) with itself. The centre manifold theory will show instead that the pertinent interaction is between the

fundamental mode and its first overtone. Since modes other than the fundamental are stable at and near $\tilde{R}_c$, we seek an expansion of the two-dimensional centre manifold for the stable modes with indices l at $\tilde{R}/\tilde{R}_c = 1$:

$$A_l = h_l(A_1, A_1^*) \quad l \neq 1,$$

where $h_l \sim O(|A_1|^2)$ and substitute this into the amplitude equation for A_1. We shall retain up to $O(|A_1|^3)$ terms which is the lowest order necessary to determine the amplitude of the roll. To this order of resolution, the only nonlinear term in the A_1 equation that contributes is $A_1^* A_2$ while the other nonlinear terms are $O(|A_1|^4)$. Consequently, near $\tilde{R}_c$ and to $O(3)$ in the amplitude of the roll solution, the only pertinent equations are

$$\frac{dA_1}{dt} = d_1 A_1 + \hat{R}_c P[2, -1] A_1^* A_2, \tag{5.2a}$$

$$\frac{dA_2}{dt} = d_2 A_2 + \hat{R}_c P[1, 1] A_1^2, \tag{5.2b}$$

where $\hat{R}_c$ is actually R_c but we shall retain the $\hat{\mathrm{L}}$ for now. The extended centre manifold for $\tilde{R}$ near $\tilde{R}_c$ is then to leading order (see Carr 1981 and Guckenheimer & Holmes 1983 for derivations)

$$A_2 = -\hat{R}_c P[1, 1] A_1^2 / d_2^c + O(|A_1|^4, |1 - \tilde{R}/\tilde{R}_c| \, |A_1|^2), \tag{5.3}$$

where d_2^c denotes the growth rate of the first overtone at $\tilde{R} = \tilde{R}_c$, and all other modes are negligible in the present resolution. Note that R is evaluated at R_c (and $\tilde{R}$ and $\tilde{R}_c$) for this local theory. Substituting (5.3) into (5.2a) yields the following leading-order amplitude equation near $\tilde{R}_c$, which is essentially the classical Stuart–Landau equation:

$$\frac{dA_1}{dt} = d_1 A_1 - \hat{R}_c^2 P[1, 1] P[2, -1] \, |A_1|^2 A_1 / d_2^c + O(|A_1|^5, |1 - \tilde{R}/\tilde{R}_c| \, |A_1|^3). \tag{5.4}$$

Although the linear growth rate of (5.4) is valid for all $\tilde{R}$ because of (3.17), the centre manifold theory is only valid if $d_1 \sim O(|1 - \tilde{R}/\tilde{R}_c|) \ll 1$. This then imposes a constraint on the region of validity of (5.4). It is only valid if the omitted terms are smaller than $d_1 A_1$, namely

$$|A_1| \sim O(|1 - \tilde{R}/\tilde{R}_c|^{\frac{1}{2}})$$

and hence $|1 - \tilde{R}/\tilde{R}_c|$ must be small and we are restricted to a neighbourhood of $\tilde{R}_c$. We have hence derived the Stuart–Landau equation using centre manifold theory. In this original version of the centre manifold theory, d_1 is expanded to leading order, namely linear, in $1 - \tilde{R}/\tilde{R}_c$ such that the linear growth term is of $O(|A_1|^3)$. However, Roberts (1989) has recently pointed out that, since the omitted terms are of $O(|A_1|^5)$ or (as in most cases) even higher, one could actually expand d_1 to $O(|1 - \tilde{R}/\tilde{R}_c|^{\frac{3}{2}})$. For the same reason, $\hat{R}^2/d_2$ in the nonlinear interaction term does not have to be evaluated at the critical point but can be expanded to the next order in $|1 - \tilde{R}/\tilde{R}_c|^{\frac{1}{2}}$. In this analysis, we shall adopt Roberts' invariant manifold approach and will in fact relax these restrictions all together and evaluate the actual values of d_1, R_c and d_2 along path (3.17). This is, of course, only consistent with the omitted terms in (5.4) if we are near the critical point. The resulting equation is then

$$\frac{dA_1}{dt} = d_1 A_1 - \hat{R}^2 P[1, 1] P[2, -1] \, |A_1|^2 A_1 / d_2. \tag{5.5}$$

Consider a polar coordinate transform

$$A_1 = r_1 \exp(i\theta_1). \tag{5.6}$$

Equation (5.5) is then transformed to

$$\frac{\mathrm{d}r_1}{\mathrm{d}t} = \{d_1 - \hat{R}^2 P[1,1]P[2,-1]\, r_1^2/d_2\}\, r_1, \tag{5.7a}$$

$$\frac{\mathrm{d}\theta_1}{\mathrm{d}t} = 0. \tag{5.7b}$$

From tables 3 and 5, d_1 is positive for $\tilde{R} > \tilde{R}_c$, d_2 is negative (since the superharmonic is stable near $\tilde{R}_c$) and $P[1,1]P[2,-1]$ is negative for $Pr = 5.5$. Hence, the primary roll solution, which is a mixed-mode solution since it contains both the fundamental and its first overtone, bifurcates supercritically at $\tilde{R}_c$ and the amplitude of its fundamental α_c mode is

$$r_1 = \left|\frac{d_1 d_2}{\hat{R}^2 P[1,1]P[2,-1]}\right|^{\frac{1}{2}} = \left|\frac{d_1 d_2}{P[1,1]P[2,-1]}\right|^{\frac{1}{2}} \frac{\tan\theta}{\tilde{R}_c(\tilde{R}/\tilde{R}_c)^{\frac{1}{2}}}, \tag{5.8a}$$

which shows that the roll amplitude increases with θ due to the increasing normal amplitude of the buoyancy force. The amplitude of the superharmonic mode in the primary roll is given by the centre manifold projection of (5.3),

$$r_2 = \left|\frac{d_1}{\hat{R}P[2,-1]}\right|. \tag{5.8b}$$

Hence, the amplitude ratio in the primary roll near $\tilde{R}_c$ is

$$r_2/r_1 = |d_1/d_2|^{\frac{1}{2}} |P[1,1]/P[2,-1]|^{\frac{1}{2}} \tag{5.8c}$$

which is independent of θ. Note that the first overtone mode r_2 of the main flow is actually linearly stable near $\tilde{R}_c$. It has been excited through nonlinear interaction to dissipate energy from the fundamental. This interaction between the fundamental and the first overtone also determines the direction and stability of the primary roll solution that bifurcates from $\tilde{R}_c$. A simple analysis of (5.7*a*) reveals that if $P[1,1]P[2,-1]$ is negative as in the present problem, the bifurcation is supercritical and the solution is stable to disturbances with wavenumber α_*. If $P[1,1]P[2,-1]$ is positive, the bifurcation is subcritical and the new solution is unstable. The term $\hat{R}P[1,1]P-2,-1]/d_2$ is the Landau constant of the Stuart–Landau equation if it is evaluated at the critical point.

The above techniques can also be applied in regions on path (3.17) where other modes of the basic flow become neutrally stable. However, at these points, the fundamental mode $m = 1$ and possibly others have already destabilized and there are hence more than one dominant (master) mode. The centre-unstable manifold techniques of carrying out these expansions are identical to those of the centre manifold expansion and they have been described in detail by Armbruster *et al.* (1989). For example, Armbruster *et al.* (1989) have shown that the travelling wave instability of the primary roll solution occurs when the first overtone of the basic flow is nearly unstable, $d_2 \sim 0$. This allows us to study the secondary instability of a finite-amplitude primary solution with amplitude equations derived with the basic flow as the reference point. Since there are now two dominant modes, the fundamental and the first overtone, and since the subharmonics are ignored here, the centre-unstable manifold expansion involves only one overtone ($m = 3$),

$$\begin{aligned} A_3 &= h_3(A_1, A_1^*, A_2, A_2^*) \\ &= -\hat{R}P[1,2]A_1 A_2/(d_3 - d_1). \end{aligned} \tag{5.9}$$

Note that, as before, we do not evaluate $\hat{R}$, d_3 and d_1 at the point where d_2 vanishes exactly but follow Roberts in retaining their $\tilde{R}$ dependence. It is understood, of course, that (5.9) is only valid near this point. Upon substituting (4.9) into the evolution equations of A_1 and A_2, one obtains the two complex amplitude equations which determine the interaction between the fundamental and its overtone away from $\tilde{R}_c$ and near $d_2 = 0$ on path (3.17), which occurs at very large $\tilde{R}$ values,

$$\frac{dA_1}{dt} = A_1(d_1 - a_1|A_2|^2) + \hat{R}P[-1,2]A_1^* A_2, \tag{5.10a}$$

$$\frac{dA_2}{dt} = A_2(d_2 - a_2|A_1|^2) + \hat{R}P[1,1]A_1^2, \tag{5.10b}$$

where

$$a_1 = \hat{R}^2 P[-2,3]P[1,2]/(d_3 - d_1), \quad a_2 = \hat{R}^2 P[-1,3]P[1,2]/(d_3 - d_1).$$

Comparing (5.10) to (5.2), it is clear that the terms a_1 and a_2, which arise from projection of the A_3 dynamics, become important away from $\tilde{R}_c$. Introducing polar coordinates as before

$$A_l = r_l \exp(i\theta_l) \tag{5.11}$$

and the phase difference

$$\phi = 2\theta_1 - \theta_2 \tag{5.12}$$

one obtains the following evolution equations for the amplitude and the phase lag:

$$\frac{dr_1}{dt} = r_1(d_1 - a_1 r_2^2) + \hat{R}P[-1,2]r_1 r_2 \cos\phi, \tag{5.13a}$$

$$\frac{dr_2}{dt} = r_2(d_2 - a_2 r_1^2) + \hat{R}P[1,1]r_1^2 \cos\phi, \tag{5.13b}$$

$$\frac{d\phi}{dt} = -\hat{R}(2P[-1,2]r_2 + P[1,1]r_1^2/r_2)\sin\phi. \tag{5.13c}$$

Note that

$$\frac{d\theta_1}{dt} = -\hat{R}P[-1,2]r_2 \sin\phi, \quad \frac{d\theta_2}{dt} = \hat{R}P[1,1](r_1^2/r_2)\sin\phi \tag{5.14}$$

such that a fixed point of (5.13) with vanishing $\sin\phi$ implies that θ_1 and θ_2 are constant and the fixed point corresponds to a steady solution (standing roll) from (5.11). On the other hand, if $\sin\phi$ does not vanish for a fixed point, θ_1 and θ_2 vary linearly with time and it corresponds to a travelling roll. It is an easy calculation to determine the fixed points of (5.13). The primary standing roll solution, which was approximated by (5.8) near $\tilde{R}_c$, now takes the following form:

$$\sin\phi = 0, \quad \cos\phi = -1, \tag{5.15a}$$

$$r_2 = \{-\hat{R}P[-1,2] + (\hat{R}^2 P[-1,2]^2 + 4a_1 d_1)^{\frac{1}{2}}\}/2a_1, \tag{5.15b}$$

$$r_1 = \{r_2 d_2/(\hat{R}P[1,1] + r_2 a_2)\}^{\frac{1}{2}}. \tag{5.15c}$$

Note that while (5.15c) reduces to (5.8a) after substituting (5.8b) as a_2 vanishes, (5.15b) is singular in this limit. The content of the overtone in the primary roll is so high that it escapes the local approximation of (5.2) and (5.4). It is seen from (5.15a) that the fundamental and the superharmonic modes of the standing roll solution have a phase shift of π away from $\tilde{R}_c$. This is also consistent with our numerical result of table 6. The previous local analysis near $\tilde{R}_c$ could not decipher this phase shift (see (5.7b)).

It is striking that the travelling roll solution with a non-vanishing $\sin\phi$ can be easily derived from the phase equation (5.13*c*) to yield the amplitude ratio

$$r_2/r_1 = |P[1,1]/2P[-1,2]|^{\frac{1}{2}} \tag{5.16}$$

which is true for all R and θ! The estimated value from (5.16) is 1.019. Consequently, to leading order, when the amplitude ratio of the primary roll solution reaches the critical value of (5.16), it becomes unstable to travelling roll instability. The resulting travelling roll then retains this amplitude ratio for all subsequent R. Although we did not compute this travelling roll solution numerically in the previous section because such a spanwise-propagating wave has not been observed, it is clear from table 6 that our primary roll solution has already been destabilized by subharmonic disturbances when $r_2/r_1 = 0.786$. The travelling wave instability of Armbruster *et al.* (1989), which occurs at $r_2/r_1 = 1.019$, is hence irrelevant to the present problem and we shall focus on the observed and computed subharmonic instability. Nevertheless, the above analysis involving the phase equations of (5.14) implies that standing roll and travelling wave solutions correspond to different phase resonances. For a standing roll, $\mathrm{d}\theta_m/\mathrm{d}t$ must vanish for all dominant modes and (5.14) implies that $\sin\phi = 0$. For a wave travelling at constant speed, $\mathrm{d}\theta_m/\mathrm{d}t$ is a non-zero constant and $\sin\phi$ must be a non-zero constant. Hence, a standing roll that does not propagate possesses a very unique phase resonance between its dominant modes. This will also be true for the standing rolls after they have merged in the presence of subharmonic instabilities.

At $\tilde{R}_{\frac{1}{2}}$ on path (3.17) in figure 8, the fundamental and the subharmonic modes of the basic flow have already destabilized. However, the $\frac{3}{2}$ mode is also nearly unstable with a growth rate of $d_{\frac{3}{2}} = -0.08$. Consequently, all three modes are dominant. We shall derive the master equations for these modes to study the interaction between the $\frac{1}{2}$ and $\frac{3}{2}$ modes. However, it is understood that if other paths closer to the neutral curves in figure 8 are taken, either the $\frac{1}{2}$ or the $\frac{3}{2}$ mode becomes stable and the equations can be further reduced. Also, unlike the travelling wave instability, the first overtone ($m = 2$) is now stable. The expansions are then

$$A_2 \sim -\hat{R}\left\{\frac{P[1,1]A_1^2}{d_2-2d_1} + \frac{P[\frac{1}{2},\frac{3}{2}]A_{\frac{1}{2}}A_{\frac{3}{2}}}{d_2-d_{\frac{1}{2}}-d_{\frac{3}{2}}}\right\} \tag{5.17a}$$

$$A_{\frac{5}{2}} \sim -\hat{R}\frac{P[1,\frac{3}{2}]A_1A_{\frac{3}{2}}}{d_{\frac{5}{2}}-d_1-d_{\frac{3}{2}}}, \tag{5.17b}$$

$$A_3 \sim -\hat{R}\frac{P[\frac{3}{2},\frac{3}{2}]A_{\frac{3}{2}}^2}{d_3-2d_{\frac{3}{2}}}. \tag{5.17c}$$

We note that, unlike the expansion near $\tilde{R}_c$ in (5.3), d_1 does not vanish there and $A_{\frac{1}{2}}$ and $A_{\frac{3}{2}}$ have become dominant modes. Substituting (5.17) into (5.1) then yields the master equations for modes 1, $\frac{1}{2}$ and $\frac{3}{2}$,

$$\frac{\mathrm{d}A_1}{\mathrm{d}t} = \{d_1+T_1|A_1|^2+T_2|A_{\frac{1}{2}}|^2+T_3|A_{\frac{3}{2}}|^2\}A_1+D_1A_{\frac{1}{2}}^2+D_2A_{\frac{1}{2}}^*A_{\frac{3}{2}}+T_4A_1^*A_{\frac{1}{2}}A_{\frac{3}{2}}, \tag{5.18a}$$

$$\frac{\mathrm{d}A_{\frac{1}{2}}}{\mathrm{d}t} = \{d_{\frac{1}{2}}+T_5|A_1|^2+T_6|A_{\frac{1}{2}}|^2+T_7|A_{\frac{3}{2}}|^2\}A_{\frac{1}{2}}+D_3A_{\frac{1}{2}}^*A_1+D_4A_1^*A_{\frac{3}{2}}+T_8A_{\frac{3}{2}}^*A_1^2, \tag{5.18b}$$

$$\frac{\mathrm{d}A_{\frac{3}{2}}}{\mathrm{d}t} = \{d_{\frac{3}{2}}+T_9|A_1|^2+T_{10}|A_{\frac{1}{2}}|^2+T_{11}|A_{\frac{3}{2}}|^2\}A_{\frac{3}{2}}+D_5A_{\frac{1}{2}}A_1+T_{12}A_{\frac{1}{2}}^*A_1^2, \tag{5.18c}$$

where the quadratic and cubic interaction coefficients D_i and T_i are related to the original nonlinear coefficients by

$$D_1 = \hat{R}P[\tfrac{1}{2},\tfrac{1}{2}],\quad D_2 = \hat{R}P[-\tfrac{1}{2},\tfrac{3}{2}],\quad D_3 = \hat{R}P[-\tfrac{1}{2},1],\quad D_4 = \hat{R}P[-1,\tfrac{3}{2}],$$
$$D_5 = \hat{R}P[\tfrac{1}{2},1],\quad T_1 = -\hat{R}^2P[1,1]P[-1,2]/(d_2-2d_1),\quad T_2 = 0,$$
$$T_3 = -\hat{R}^2P[-\tfrac{3}{2},\tfrac{5}{2}]P[1,\tfrac{3}{2}]/(d_{\frac{5}{2}}-d_1-d_{\frac{3}{2}}),\quad T_4 = -\hat{R}^2P[-1,2]P[\tfrac{1}{2},\tfrac{3}{2}]/(d_2-d_{\frac{1}{2}}-d_{\frac{3}{2}}),$$
$$T_5 = T_6 = 0,\quad T_7 = -\hat{R}^2P[-\tfrac{3}{2},2]P[\tfrac{1}{2},\tfrac{3}{2}]/(d_2-d_{\frac{1}{2}}-d_{\frac{3}{2}}),$$
$$T_8 = -\hat{R}^2P[-\tfrac{3}{2},2]P[1,1]/(d_2-2d_1),\quad T_9 = -\hat{R}^2P[-1,\tfrac{5}{2}]P[1,\tfrac{3}{2}]/(d_{\frac{5}{2}}-d_1-d_{\frac{3}{2}}),$$
$$T_{10} = -\hat{R}^2P[-\tfrac{1}{2},2]P[\tfrac{1}{2},\tfrac{3}{2}]/(d_2-d_{\frac{1}{2}}-d_{\frac{3}{2}}),\quad T_{11} = -\hat{R}^2P[-\tfrac{3}{2},3]P[\tfrac{3}{2},\tfrac{3}{2}]/(d_3-2d_{\frac{3}{2}}),$$
$$T_{12} = -\hat{R}^2P[-\tfrac{1}{2},2]P[1,1]/(d_2-2d_1).$$

Since $\hat{R}$ can be easily absorbed into the definition of the nonlinear coefficients $P[n,m]$, the above master equations are valid for any system with $O(2)$ symmetry, quadratic nonlinearity and three dominant modes in $\frac{1}{2}$, 1 and $\frac{3}{2}$.

The polar representation of (5.11) can be again applied to yield

$$\frac{dr_1}{dt} = \{d_1 + T_1 r_1^2 + T_3 r_{\frac{3}{2}}^2\} r_1 + D_1 r_{\frac{1}{2}}^2 \cos\phi_1 + D_2 r_{\frac{3}{2}} r_{\frac{1}{2}}^* \cos\phi_2 + T_4 r_1 r_{\frac{3}{2}} r_{\frac{1}{2}} \cos(\phi_2 - \phi_1), \tag{5.19a}$$

$$\frac{dr_{\frac{1}{2}}}{dt} = \{d_{\frac{1}{2}} + T_7 r_{\frac{3}{2}}^2\} r_{\frac{1}{2}} + D_3 r_1 r_{\frac{1}{2}} \cos\phi_1 + D_4 r_{\frac{3}{2}} r_1 \cos\phi_2 + T_8 r_1^2 r_{\frac{3}{2}} \cos(\phi_2 - \phi_1), \tag{5.19b}$$

$$\frac{dr_{\frac{3}{2}}}{dt} = \{d_{\frac{3}{2}} + T_9 r_1^2 + T_{10} r_{\frac{1}{2}}^2 + T_{11} r_{\frac{3}{2}}^2\} r_{\frac{3}{2}} + D_5 r_1 r_{\frac{1}{2}} \cos\phi_2 + T_{12} r_1^2 r_{\frac{1}{2}} \cos(\phi_2 - \phi_1), \tag{5.19c}$$

$$\frac{d\phi_1}{dt} = \frac{1}{r_1}(D_2 r_{\frac{1}{2}} r_{\frac{3}{2}} \sin\phi_2 - D_1 r_{\frac{1}{2}}^2 \sin\phi_1) + T_4 r_{\frac{1}{2}} r_{\frac{3}{2}} \sin(\phi_2 - \phi_1) - 2D_3 r_1 \sin\phi_1$$
$$- \frac{2}{r_{\frac{1}{2}}}[D_4 r_1 r_{\frac{3}{2}} \sin\phi_2 - T_8 r_1^2 r_{\frac{3}{2}} \sin(\phi_2 - \phi_1)], \tag{5.19d}$$

$$\frac{d\phi_2}{dt} = -\frac{1}{r_{\frac{3}{2}}}[D_5 r_{\frac{1}{2}} r_1 \sin\phi_2 + T_{12} r_1^2 r_{\frac{1}{2}} \sin(\phi_2 - \phi_1)]$$
$$- \frac{1}{r_1}[D_2 r_{\frac{1}{2}} r_{\frac{3}{2}} \sin\phi_2 - D_1 r_{\frac{1}{2}}^2 \sin\phi_1] - T_4 r_{\frac{1}{2}} r_{\frac{3}{2}} \sin(\phi_2 - \phi_1)$$
$$- D_3 r_1 \sin\phi_1 - \frac{1}{r_{\frac{1}{2}}}[D_4 r_1 r_{\frac{3}{2}} \sin\phi_2 - T_8 r_1^2 r_{\frac{3}{2}} \sin(\phi_2 - \phi_1)]. \tag{5.19e}$$

Like before, the three phase equations reduce to two equations for the phase differences

$$\phi_1 = \theta_1 - 2\theta_{\frac{1}{2}},\quad \phi_2 = \theta_{\frac{3}{2}} - \theta_1 - \theta_{\frac{1}{2}}, \tag{5.20a, b}$$

where

$$\frac{d\theta_1}{dt} = -D_1 r_{\frac{1}{2}}^2 \sin\phi_1 / r_1 + D_2 r_{\frac{1}{2}} r_{\frac{3}{2}} \sin\phi_2 / r_1 + T_4 r_{\frac{1}{2}} r_{\frac{3}{2}} \sin(\phi_2 - \phi_1), \tag{5.21a}$$

$$\frac{d\theta_{\frac{1}{2}}}{dt} = \frac{1}{r_{\frac{1}{2}}}[D_3 r_1 r_{\frac{1}{2}} \sin\phi_1 + D_4 r_1 r_{\frac{3}{2}} \sin\phi_2 - T_8 r_1^2 r_{\frac{3}{2}} \sin(\phi_2 - \phi_1)], \tag{5.21b}$$

$$\frac{d\theta_{\frac{3}{2}}}{dt} = -\frac{1}{r_{\frac{3}{2}}}[D_5 r_{\frac{1}{2}} r_1 \sin\phi_2 + T_{12} r_1^2 r_{\frac{1}{2}} \sin(\phi_2 - \phi_1)]. \tag{5.21c}$$

One can decipher some important properties of standing roll solutions without solving (5.19) explicitly. For the standing solutions, the phase evolution in (5.21) must again vanish exactly. Consequently, for a subharmonic roll with negligible $\frac{3}{2}$-mode contribution, (5.21) implies a certain phase resonance among all three dominant modes

$$\sin\phi_1 = \sin\phi_2 = 0. \tag{5.22}$$

However, from (5.19*b*), since $D_3 = 2\hat{R}P[-\frac{1}{2}, 1]$ is positive from table 5 and $d_{\frac{1}{2}}$ is positive in the region where the subharmonic roll exists, the subharmonic roll with no $\frac{3}{2}$-mode contribution is a standing one if and only if $\cos\phi_1$ is negative. Hence, from (5.22), one concludes that

$$\phi_1 = \pi, \tag{5.23}$$

which is consistent with our numerical result in table 6 that there is a $\frac{1}{2}\pi$ spatial phase shift between the rolls prior and after coalescence at $\tilde{R}_{\frac{1}{2}}$, as shown schematically in figure 1. In general, the sign of the nonlinear coefficient $P[-\frac{1}{2}, 1]$ determines this phase shift. If $P[-\frac{1}{2}, 1]$ is negative, the standing rolls do not shift spatially after coalescence. Physically, with negligible contribution from the $\frac{3}{2}$ mode, the D_3 term in (5.19*b*) is the only nonlinear dissipation term which arrests the linear growth rate of the subharmonic mode. It must hence be negative such that energy can be transferred to the fundamental mode to form a saturated subharmonic roll. The fundamental, which is also linearly unstable, transfers the energy in turn to its stable overtone through nonlinear interaction.

To estimate $\tilde{R}_{\frac{1}{2}}$ and the amplitude ratio r_2/r_1, it is necessary to return to the complex amplitude equations of (5.18). The polar representation (5.19) is singular when $r_{\frac{1}{2}}$ or $r_{\frac{3}{2}}$ vanishes and is hence unsuitable for linearizing about the primary roll solution. We shall linearize (5.18) about

$$\begin{pmatrix} A_1 \\ A_{\frac{1}{2}} \\ A_{\frac{3}{2}} \end{pmatrix} = \begin{pmatrix} A_1^s \\ 0 \\ 0 \end{pmatrix} \tag{5.24}$$

where the amplitude of the primary roll $|A_1^s|^2 = r_1^2$ is derived from (5.19*a*) as

$$r_1^2 = -\frac{d_1}{T_1} = \frac{d_1(d_2 - 2d_1)}{\hat{R}^2 P[1,1]P[-1,2]}. \tag{5.25}$$

This estimate is favourably compared to the numerical values in figure 10,. The phase θ_1 will not be relevant. The resulting linearized equations are then

$$\frac{\mathrm{d}}{\mathrm{d}t}\hat{A}_1 = (d_1 + 3T_1 r_1^2)\hat{A}_1, \tag{5.26a}$$

$$\frac{\mathrm{d}}{\mathrm{d}t}A_{\frac{1}{2}} = d_{\frac{1}{2}}A_{\frac{1}{2}} + D_3 r_1 A_{\frac{1}{2}}^* + D_4 r_1 A_{\frac{3}{2}} + T_8 r_1^2 A_{\frac{3}{2}}^*, \tag{5.26b}$$

$$\frac{\mathrm{d}}{\mathrm{d}t}A_{\frac{3}{2}} = (d_{\frac{3}{2}} + T_9 r_1^2)A_{\frac{3}{2}} + D_5 r_1 A_{\frac{1}{2}} + D_{12} r_1^2 A_{\frac{1}{2}}^*, \tag{5.26c}$$

where $\hat{A}_1 = A_1 - A_1^s$. The deviation variable $\hat{A}_1$ of the fundamental mode in (5.26*a*) is decoupled from $A_{\frac{1}{2}}$ and $A_{\frac{3}{2}}$. Insofar as $T_1 r_1^2 = -d_1$ from (5.25), the eigenvalue corresponding to (5.26*a*) is $-2\mathrm{d}_1 < 0$. This simply reflects the earlier result that a

supercritical solution is stable to disturbances of its own wavelength. The linearized dynamics of the $\frac{1}{2}$ and $\frac{3}{2}$ modes then determines the stability of the primary roll with respect to the $\frac{1}{2}$ and $\frac{3}{2}$ subharmonic disturbances. Their equations in (5.26*b*) and (5.26*c*) along with their conjugates yield the Jacobian

$$\boldsymbol{J} = \begin{pmatrix} d_{\frac{1}{2}} & D_3 r_1 & D_4 r_1 & T_8 r_1^2 \\ D_3 r_1 & d_{\frac{1}{2}} & T_8 r_1^2 & D_4 r_1 \\ D_5 r_1 & T_{12} r_1^2 & d_{\frac{3}{2}} + T_9 r_1^2 & 0 \\ T_{12} r_1^2 & D_5 r_1 & 0 & d_{\frac{3}{2}} + T_9 r_1^2 \end{pmatrix}. \tag{5.27}$$

Owing to the various symmetries of the 2×2 submatrices in $\boldsymbol{J}$, it can be readily shown that $\boldsymbol{J}$ is similar to the block-diagonal matrix

$$\begin{pmatrix} \boldsymbol{J}_1 & 0 \\ 0 & \boldsymbol{J}_2 \end{pmatrix},$$

where

$$\boldsymbol{J}_1 = \begin{pmatrix} d_{\frac{1}{2}} + D_3 r_1 & D_4 r_1 + T_8 r_1^2 \\ D_5 r_1 + T_{12} r_1^2 & d_{\frac{3}{2}} + T_9 r_1^2 \end{pmatrix}, \tag{5.28a}$$

$$\boldsymbol{J}_2 = \begin{pmatrix} d_{\frac{1}{2}} - D_3 r_1 & D_4 r_1 - T_8 r_1^2 \\ D_5 r_1 - T_{12} r_1^2 & d_{\frac{3}{2}} + T_9 r_1^2 \end{pmatrix}. \tag{5.28b}$$

The stability conditions then become $\operatorname{trace} \boldsymbol{J}_1 < 0$, $\operatorname{trace} \boldsymbol{J}_2 < 0$, $\det \boldsymbol{J}_1 > 0$ and $\det \boldsymbol{J}_2 > 0$, which are very cumbersome to analyse. Simplification can be made, however, if one expands the traces and determinants of $\boldsymbol{J}_1$ and $\boldsymbol{J}_2$ about the resonant point of

$$d_1 = d_{\frac{1}{2}} = 0, \tag{5.29}$$

which is where $\tilde{R}_{\frac{1}{2}}$ emanates from the neutral curve in figure 8. In the neighbourhood of this point where $|d_1| \sim |d_{\frac{1}{2}}| \sim \boldsymbol{O}(|r_1|^2)$, which defines the size of this neighbourhood,

$$\operatorname{trace} \boldsymbol{J}_1 \sim d_{\frac{3}{2}} + O(|r_1|) < 0,$$
$$\operatorname{trace} \boldsymbol{J}_2 \sim d_{\frac{3}{2}} + O(|r_1|) < 0,$$

and hence both trace conditions are satisfied and one needs only to examine the determinant conditions. Since $|d_{\frac{3}{2}}| \gg |d_{\frac{1}{2}}| \sim O(|r_1|^2)$ in this neighbourhood, the two determinants can be shown to be related by

$$\det \boldsymbol{J}_2 = \det \boldsymbol{J}_1 - 2 D_3 d_{\frac{3}{2}} |r_1|. \tag{5.30}$$

Since $d_{\frac{3}{2}}$ is negative near the resonant point (5.29) and D_3 is positive in the present problem, $\det \boldsymbol{J}_2 > \det \boldsymbol{J}_1$ and the tightest bound is given implicitly by a vanishing

$$\det \boldsymbol{J}_2 = (d_{\frac{1}{2}} - D_3 r_1)(d_{\frac{3}{2}} + T_9 r_1^2) - (D_4 r_1 - T_8 r_1^2)(D_5 r_1 - T_{12} r_1^2) \sim (d_{\frac{1}{2}} - D_3 r_1) d_{\frac{3}{2}} - D_4 D_5 r_1^2, \tag{5.31}$$

where $d_{\frac{1}{2}}$ and $d_{\frac{3}{2}}$ vary with $\tilde{R}$ along (3.17) and so does r_1 according to (5.25). Although an explicit analytical estimate for $\tilde{R}_{\frac{1}{2}}$ cannot be written down, one sees from (5.31) that

$$d_{\frac{1}{2}} \sim D_3 r_1 + \frac{D_4 D_5 r_1^2}{d_{\frac{3}{2}}},$$

and since D_3 and D_4 are positive while D_5 and $d_{\frac{3}{2}}$ are negative from table 5, one concludes that $d_{\frac{1}{2}}(\tilde{R}_{\frac{1}{2}})$ is positive and hence the primary roll is unstable to subharmonic

disturbances after the subharmonic mode of the basic flow has destabilized. Our estimates of $\tilde{R}_{\frac{1}{2}}$ from (5.31) yields 46.5 which is very close to the numerical value of 41.0 along path (3.17). One can also estimate the amplitude ratio r_2/r_1 from (5.25) and (5.17*a*) with $A_{\frac{3}{2}} = 0$ after $\tilde{R}_{\frac{1}{2}}$ has been estimated. We obtain a value of 0.730 which is also close to the exact value of 0.786 in table 6. Condition (5.31) is, of course, only valid for paths like (3.17) which lie close to the resonant point on the right neutral curve. A similar expansion can be carried out, however, near the resonant point $d_1 = d_{\frac{3}{2}} = 0$ for paths near the left neutral curve.

6. Summary and discussion

We have constructed finite-amplitude longitudinal rolls in an inclined free-convection boundary layer and showed that they first become unstable downstream from the leading edge to static disturbances with spanwise wavelength twice that of the primary rolls. This subharmonic instability causes the adjacent rolls to merge. The $\frac{1}{2}$ mode in the secondary roll also has a spatial phase shift relative to the primary 1 mode such that an asymmetric dislocation of the rolls occurs beyond the transition. This shift is shown to be caused by a positive interaction coefficient D_3 which governs the contribution to the $A_{\frac{1}{2}}$ mode dynamics from the nonlinear interaction between the $\frac{1}{2}$ and 1 modes. A negative D_3, which may occur at other Pr values and definitely for other systems, will not induce a phase shift. Our analysis also reveals that the superharmonic travelling wave instability of the primary roll, which had been discovered by Armbruster *et al.* (1989), is generally preceded by the subharmonic instability studied here. Since path (3.17) of the present system in figure 8 skirts the Eckhaus bound (1.1), the subharmonic instability also precedes sideband instability. Consequently, one expects subharmonic instability, which includes $\tilde{R}_{\frac{3}{2}}$ and $\tilde{R}_{\frac{1}{2}}$ in figure 8, to be a dominant instability of primary rolls in many non-dispersive systems with $O(2)$ symmetry.

The ultimate physical manifestation of the subharmonic instability occurring in the flow studied here is a pinching (or dislocation) phenomenon similar to a propagating wavenumber adjustment mechanism observed by Busse & Whitehead (1971; see their figure 15) for supercritical Rayleigh–Bénard convection. Here, the adjustment takes place spatially in the steady state, and so we cannot describe the local details of the adjustment on the basis of the present approach. A considerable amount of work (for a recent review, see Walgraef & Ghoniem 1990) has been devoted to the study of dislocations, including some research relevant to Rayleigh–Bénard convection (e.g. Cross & Newell 1984). Most of this work is based on model one-dimensional amplitude equations which might be applicable here if the adjustment were sufficiently gradual. However, as indicated in figure 1, the region over which the adjustment occurs is comparable to the wavelength of the primary roll, and so the direct relevance of such results is not yet clear.

The saddle-node annihilation of the subharmonic standing rolls at $\tilde{R}_t$ is an instability of the secondary merged rolls that is difficult to decipher from the master amplitude equations for modes 1, $\frac{3}{2}$ and $\frac{1}{2}$, such as those derived in §5 and those by Janssen (1986) for sheared waves and Kelly (1967) for free shear layers. Instead, a numerical analysis with a large number of modes, such as that in §4, is carried out. It is also interesting that no stable low-dimensional attractors exist beyond $\tilde{R}_t$ and an irregular temporal behaviour is obtained. This is quite distinct from the intermittent bursts obtained at the heteroclinic bifurcation of the superharmonic travelling wave as shown by Armbruster *et al.* (1988) for generic $O(2)$ systems

without subharmonics and by Aubry *et al.* (1988) or bursts in turbulent boundary layers. Also, as Aubry *et al.* (1988) explained in their use of large-scale empirical eigenfunctions, irregular temporal behaviour of our model and theirs can only be associated with large-scale structures since only a small number of modes with wavenumbers close to α_c are used. If the observed fluctuation is associated with fine structures and large wavenumbers, it cannot be described by these low-dimensional models.

Finally, we remark that, while Armbruster *et al.* (1989) were able to study a rather generic unfolding of the two mode equations in (5.10) for systems with $O(2)$ symmetry and uncover travelling wave instability and other phenomena, the same general analysis is unlikely for the three mode equations (5.18) of subharmonic instabilities because of the large number of independent parameters. Some analysis is, however, possible if either $A_{\frac{1}{2}}$ or $A_{\frac{3}{2}}$ becomes stable as one traverses along the left or right neutral curves, respectively. This will appear in a separate manuscript.

This work was supported by the National Science Foundation under Grant No. ENG-8451116 and by the Center of Applied Mathematics at the University of Notre Dame. We are also grateful to M. Cheng for his assistance in the derivation of the amplitude equations.

Appendix. The effect of mean flow interaction

The centre-unstable manifold theory of §5 can be used to show that mean flow interaction does not change our estimate for the onset of subharmonic instability to leading order. Including the $m = 0$ mode in (5.1), one obtains

$$\frac{dA_0}{dt} = [\ldots] + \hat{R}P[0,0]A_0^2, \qquad \frac{dA_{\frac{1}{2}}}{dt} = [\ldots] + \hat{R}P[\tfrac{1}{2},0]A_{\frac{1}{2}}A_0,$$

$$\frac{dA_1}{dt} = [\ldots] + \hat{R}P[1,0]A_1A_0, \quad \frac{dA_{\frac{3}{2}}}{dt} = [\ldots] + \hat{R}P[\tfrac{3}{2},0]A_{\frac{3}{2}}A_0,$$

$$\frac{dA_2}{dt} = [\ldots] + \hat{R}P[2,0]A_2A_0, \quad \frac{dA_{\frac{5}{2}}}{dt} = [\ldots] + \hat{R}P[\tfrac{5}{2},0]A_{\frac{5}{2}}A_0,$$

$$\frac{dA_3}{dt} = [\ldots] + \hat{R}P[3,0]A_3A_0,$$

where $[\ldots]$ denotes the original terms in (5.1). Note also that A_0 is a real amplitude $A_0 = A_0^*$. Since A_0 is always stable, it must also be expanded in terms of the nearly neutral and unstable modes, A_1, $A_{\frac{1}{2}}$ and $A_{\frac{3}{2}}$. However, to second order in these modes, the expansions of A_2, $A_{\frac{5}{2}}$ and A_3 remain the same as those in (5.17). The only addition to the final amplitude equation of (5.18) is

$$A_0 \sim -\hat{R}\left\{\frac{P[1,-1]A_1A_1^*}{d_0-2d_1} + \frac{P[\frac{1}{2},-\frac{1}{2}]A_{\frac{1}{2}}A_{\frac{1}{2}}^*}{d_0-2d_{\frac{1}{2}}} + \frac{P[\frac{3}{2},-\frac{3}{2}]A_{\frac{3}{2}}A_{\frac{3}{2}}^*}{d_0-2d_{\frac{3}{2}}}\right\}.$$

Substituting this expansion of the zero-wavenumber mode and those for the other stable modes in (5.17) into the amplitude equations of A_1, $A_{\frac{1}{2}}$ and $A_{\frac{3}{2}}$ in (5.1), one still

obtains (5.18) but some of the cubic coefficients T_i are now altered by the mean flow interaction:

$$T_1 = -\hat{R}^2\left\{\frac{P[1,1]P[-1,2]}{d_2-2d_1}+\frac{P[1,0]P[1,-1]}{d_0-2d_1}\right\},\quad T_2 = -\hat{R}^2\frac{P[1,0]P[\frac{1}{2},-\frac{1}{2}]}{d_0-2d_{\frac{1}{2}}},$$

$$T_3 = -\hat{R}^2\left\{\frac{P[-\frac{3}{2},\frac{5}{2}]P[1,\frac{3}{2}]}{d_{\frac{1}{2}}-d_1-d_{\frac{3}{2}}}+\frac{P[1,0]P[\frac{3}{2},-\frac{3}{2}]}{d_0-2d_{\frac{3}{2}}}\right\},\quad T_5 = -\hat{R}^2\frac{P[\frac{1}{2},0]P[1,-1]}{d_0-2d_1},$$

$$T_6 = -\hat{R}^2\frac{P[\frac{1}{2},0]P[\frac{1}{2},-\frac{1}{2}]}{d_0-2d_{\frac{1}{2}}},\quad T_7 = -\hat{R}^2\left\{\frac{P[-\frac{3}{2},2]P[\frac{1}{2},\frac{3}{2}]}{d_2-d_{\frac{1}{2}}-d_{\frac{3}{2}}}+\frac{P[\frac{1}{2},0]P[\frac{3}{2},-\frac{3}{2}]}{d_0-2d_{\frac{3}{2}}}\right\},$$

$$T_9 = -\hat{R}^2\left\{\frac{P[-1,\frac{5}{2}]P[1,\frac{3}{2}]}{d_{\frac{1}{2}}-d_1-d_{\frac{3}{2}}}+\frac{P[\frac{3}{2},0]P[1,-1]}{d_0-2d_1}\right\},$$

$$T_{10} = -\hat{R}^2\left\{\frac{P[-\frac{1}{2},2]P[\frac{1}{2},\frac{3}{2}]}{d_2-d_{\frac{1}{2}}-d_{\frac{3}{2}}}+\frac{P[\frac{3}{2},0]P[\frac{1}{2},-\frac{1}{2}]}{d_0-2d_{\frac{1}{2}}}\right\},$$

$$T_{11} = -\hat{R}^2\left\{\frac{P[-\frac{3}{2},3]P[\frac{3}{2},\frac{3}{2}]}{d_3-2d_{\frac{3}{2}}}+\frac{P[\frac{3}{2},0]P[\frac{3}{2},-\frac{3}{2}]}{d_0-2d_{\frac{3}{2}}}\right\}.$$

These cubic coefficients will after some of the elements of the matrix $\boldsymbol{J}$ in (5.27) although the two zero elements remain unchanged. The two block diagonal matrices in (5.28) also have the same expressions but with the new T_i coefficients. As a result, the leading-order estimate of $\hat{R}_{\frac{1}{2}}$ in (5.31), which involves only the quadratic terms, remains the same as before.

REFERENCES

ARMBRUSTER, D., GUCKENHEIMER, J. & HOLMES, P. 1988 Heteroclinic cycles and modulated travelling waves in systems with $O(2)$ symmetry. *Physica* **29D**, 257–282.

ARMBRUSTER, D., GUCKENHEIMER, J. & HOLMES, P. 1989 Kuramoto–Sivashinsky dynamics on the center-unstable manifold. *SIAM J. Appl. Maths* **49**, 676–691.

AUBRY, N., HOLMES, P., LUMLEY, J. L. & STONE, E. 1988 The dynamics of coherent structures in the wall region of a turbulent boundary layer. *J. Fluid Mech.* **192**, 115–173.

BENNEY, D. J. 1960 A nonlinear theory for oscillations in a parallel flow. *J. Fluid Mech.* **10**, 209–236.

BENNY, D. J. & LIN, C. C. 1960 On secondary motion induced by oscillations in a shear flow. *Phys. Fluids* **3**, 656–657.

BUSSE, F. H. & OR, A. C. 1986 Subharmonic and asymmetric convection rolls. *Z. Angew. Math. Phys.* **37**, 608–623.

BUSSE, F. H. & WHITEHEAD, J. A. 1971 Instabilities of convection rolls in a high Prandtl number fluid. *J. Fluid Mech.* **47**, 305–320.

CANUTO, C., HUSSAINI, M. Y., QUARTERONI, A. & ZANG, T. A. 1988 *Spectral Methods in Fluid Dynamics*. Springer.

CARR, J. 1981 *Application of Center Manifold Theory*. Springer.

CARR, J. & MUNCASTER, R. G. 1983 The application of centre manifolds to amplitude expansions. *J. Diffl Equat.* **50**, 260–279.

CHEN, L. H. & CHANG, H.-C. 1986 Nonlinear waves on liquid film surfaces – II. Bifurcation analysis of the long wave equation. *Chem. Engng Sci.* **41**, 2477–2486.

CHEN, T. S. & TZUOO, K. L. 1982 Vortex instability of free convection flow over horizontal and inclined surfaces. *Trans. ASME* C: *J. Heat Transfer* **104**, 637–643.

CHENG, M. & CHANG, H.-C. 1990 A generalized sideband stability theory via center manifold projection. *Phys. Fluids* A **2**, 1364–1379.

CLEVER, R. M., BUSSE, F. H. & KELLY, R. E. 1977 Instabilities of longitudinal convection rolls in Couette flow. *Z. Angew. Math. Phys.* **28**, 771–783.

CROSS, M. C. & NEWELL, A. C. 1984 Convection patterns in large aspect ratio systems. *Physica* **10D**, 299–310.

DAUDPOTA, Q. I., HALL, P. & ZANG, T. A. 1988 On the nonlinear interaction of Görtler vortices and Tollmien–Schlichting waves in curved channel flows at finite Reynolds numbers. *J. Fluid Mech.* **193**, 569–595.

ECKHAUS, W. 1963 Problémes nonlineaires de stabilité dans un espace à deux dimensions. *J. Méc.* **2**, 153–172.

FOX, L. & PARKER, I. B. 1968 *Chebyshev Polynomials in Numerical Analysis.* Oxford University Press.

GEBHART, B., JALURIA, Y., MAHAJAN, R. L. & SAMMAKIA, B. 1988 *Buoyancy-Induced Flow and Transport.* Hemisphere.

GEBHART, B. & MAHAJAN, R. L. 1982 Instability and transition in buoyancy-induced flow. *Adv. App. Mech.* **22**, 231–314.

GILPIN, R. R., IMURA, H. & CHENG, K. C. 1978 Experiments on the onset of longitudinal vortices in horizontal Blasius flow heated from below. *Trans. ASME* C: *J. Heat Transfer* **100**, 71–77.

GOTTLIEB, D. & ORSZAG, S. A. 1977 *Numerical Analysis of Spectral Methods: Theory and Applications.* NSF-CMBS Monograph No. 25. SIAM.

GUCKENHEIMER, J. & HOLMES, P. 1983 *Nonlinear Oscillations, Dynamical Systems, and Bifurcations of Vector Fields.* Springer.

HAALAND, S. E. & SPARROW, E. M. 1973 Vortex instability of natural convection flow on inclined surfaces. *Intl J. Heat Mass Transfer* **16**, 2355–2367.

HALL, P. 1983 The linear development of Görtler vortices in a growing boundary layer. *J. Fluid Mech.* **130**, 41–58.

HO, K. L. & CHANG, H. C. 1988 On nonlinear doubly-diffusive Marangoni instability. *AIChE J.* **34**, 705–722.

HWANG, G. J. & CHENG, K. C. 1973 Thermal instability of laminar natural convection flow on inclined isothermal plates. *Can. J. Chem. Engng* **51**, 465–470.

HWANG, S. H. & CHANG, H. C. 1989 Non-Boussinesq effects on transitions in Hele-Shaw convection. *Phys. Fluids* A **1**, 924–937.

IYER, P. A. & KELLY, R. E. 1974 The stability of the laminar free convection flow induced by a heated plate. *Intl J. Heat Mass Transfer* **17**, 517–525.

JANSSEN, P. A. E. M. 1986 Period-doubling of gravity-capillary waves. *J. Fluid Mech.* **172**, 531–546.

JENSEN, K. F. 1987 Micro-reaction engineering application of reaction engineering to processing of electronic and photonic materials. *Chem. Engng Sci.* **42**, 923–958.

KAHAWITA, R. A. & MERONEY, R. N. 1974 The vortex of instability in natural convection flow along inclined plates. *Intl J. Heat Mass Transfer* **17**, 541–548.

KELLY, R. E. 1967 On the stability of an inviscid shear layer which is periodic in space and time. *J. Fluid Mech.* **27**, 657–689.

LLOYD, J. R. & SPARROW, E. M. 1970 On the instability of natural convection flow on inclined plates. *J. Fluid Mech.* **42**, 465–470.

MONKEWITZ, P. A. 1988 Subharmonic resonance, pairing and shredding in the mixing layer. *J. Fluid Mech.* **188**, 223–252.

ORSZAG, S. A. 1971 Accurate solution of the Orr–Sommerfeld stability equation. *J. Fluid Mech.* **50**, 315–335.

PROCTOR, M. R. E. & JONES, C. A. 1988 The interaction of two spatially resonant patterns in thermal convection. Part 1. Exact 1:2 resonance. *J. Fluid Mech.* **188**, 301–335.

ROBERTS, A. J. 1989 The utility of the invariant manifold description of the evolution of a dynamical systems. *SIAM J. Math. Anal.* **20**, 1447–1458.

SATO, H. 1959 Further investigation on the transition of two-dimensional separated layers at subsonic speeds. *J. Phys. Soc. Japan* **14**, 1797–1810.

SPALART, P. R. 1984 Spectral method for external viscous flow. *Contemp. Maths* **28**, 315–335.

SPARROW, E. M. & HUSAR, R. B. 1969 Longitudinal vortices in natural convection flow on inclined surfaces. *J. Fluid Mech.* **37**, 251–255.

SWEARINGEN, J. D. & BLACKWELDER, R. F. 1987 The growth and breakdown of streamwise vortices in the presence of a wall. *J. Fluid Mech.* **182**, 255–290.

SZEWCZYK, A. A. 1962 Stability and transition of the free-convection layer along a vertical flat plate. *Intl J. Heat Mass Transfer* **5**, 903–914.

THOMAS, F. O. 1990 An experimental investigation into the role of simultaneous amplitude and phase modulation in the transition of a planar jet. *Phys. Fluids* A **2**, 553–574.

TZUOO, K. L., CHEN, T. S. & ARMALY, B. F. 1985 Wave instability of natural convection flow on inclined surfaces. *Trans. ASME* C: *Heat Transfer* **107**, 107–111.

VILLADSEN, J. V. & STEWART, W. E. 1967 Solution of boundary-value problems by orthogonal collocation. *Chem. Engng Sci.* **22**, 1483–1501.

WALGRAEF, D. & GHONIEM, N. M. (EDS) 1990 *Patterns, Defects and Materials Instabilities*, NATO ASI Series E, vol. 183. Kluwer.

WALTON, I. C. 1982 On the onset of Rayleigh–Bénard convection in a fluid layer of slowly increasing depth. *Stud. Appl. Maths* **67**, 199–216.

YANG, K. T. 1960 Possible similarity solutions for laminar free convection on vertical plates and cylinders. *Trans. ASME* E: *J. Appl. Mech.* **27**, 230–236.

YANG, K. T. 1988 Transitions and bifurcations in laminar buoyant flows in confined enclosures. *Trans. ASME* C: *J. Heat Transfer* **110**, 1191–1204.